Ph.D. DISSERTATION

Atomic Layer Deposition of Germanium Telluride Thin Films Using Intermediate Precursor Formation Method for Phase-change Memory Application

by

Taehong Gwon

February 2017

DEPARTMENT OF MATERIALS SCIENCE AND ENGINEERING

COLLEGE OF ENGINEERING

SEOUL NATIONAL UNIVERSITY

Atomic Layer Deposition of Germanium Telluride Thin Films Using Intermediate Precursor Formation Method for Phase-change Memory Application

Advisor : Prof. Cheol Seong Hwang

by

Taehong Gwon

A thesis submitted to the Graduate Faculty of Seoul National University in partial fulfillment of the requirements for the Degree of Doctor of Philosophy

Department of Materials Science and Engineering

February 2017

Approved

by

Chairman of Advisory Committee : Hyeong Joon Kim

Vice-chairman of Advisory Committee : Cheol Seong Hwang

Advisory Committee : Seungwu Han

Advisory Committee : Byung Joon Choi

Advisory Committee : Taeyong Eom

Abstract

Current information technology industry requires high speed, high density, low power consumption memory devices. However, the present semiconductor industry which is represented by dynamic random access memory (DRAM) and NAND flash, has reached the limit of scaling, thus, researches on next-generation memory has been continued. Phase-change random access memory (PRAM), which records data through the resistivity difference between amorphous and crystalline phase of phase-change materials (PCM) is one of the strongest candidate for next-generation non-volatile memory. The most widely studied materials for PCM are GeTe-Sb_2Te_3 pseudobinary materials for its fast phase transition, superior retention property, and low power consumption.

Meanwhile, the early stage of researches on PCRAM has mushroom structure that forms a small electrode contact at planar PCM for its operation. However, the mushroom structured PCRAM requires improvement due to very low thermal efficiency and cross-talk issue between adjacent cells. Therefore, new structure was proposed that fills PCM into a small contact hole, called confined structure. The confined structure has become new standard of PCRAM by much higher thermal efficiency, improved cross-talk problem, and even strong resistivity on etch damage during device fabrication process. In

order to fabricate a PCRAM device with confined structure, deposition process with excellent step coverage properties became important. By the requirement, atomic layer deposition (ALD) of PCM became necessary.

Previous researches on atomic layer deposition of ternary GeSbTe materials left many challenging tasks. One of the most important issue at previous researches on GeSbTe ALD was the composition of the material, which lies on $GeTe_2$-Sb_2Te_3 tie line rather than desired GeTe-Sb_2Te_3 tie line. The problem was originated from characteristics of the Ge-precursor used in the process, wherein +4 oxidation state to form $GeTe_2$ by reaction of Te precursor with -2 oxidation state. Because the most stable oxidation state of Ge element is +4, there have been many difficulties in the development of Ge(II) precursors and the deposition process using the precursor such as polymerization of the precursor molecule by its chemical instability. In this work, novel processes for atomic layer deposition of GeTe films were suggested. In common for both processes, a newly suggested methods are used in which the form of the precursor and the molecules actually taking place in the deposition are changed.

The first process was developed using $Ge(N(Si(CH_3)_3)_2)_2$ and $((CH_3)_3Si)_2Te$ as the Ge- and Te-precursors, wherein the Ge atom has +2 oxidation state. The Ge-precursor was introduced to chamber with methanol vapor to form intermediate precursor, $Ge(OMe)_2$, which is more reactive, but has no long term stability as precursor, by gas phase reaction. The Te-precursor was also

introduced with methanol vapor to form H_2Te. The intermediate precursors described above played the role as precursors in the deposition to form GeTe films. Mechanism of chemical reactions in deposition process was studied. Combined process with previously settled Sb_2Te_3 deposition process using $Sb(OC_2H_5)_3$ and $((CH_3)_3Si)_2Te$ was also attempted.

The second process using $HGeCl_3$ and $((CH_3)_3Si)_2Te$ as the Ge- and Te-precursors was also suggested. The Ge-precursor wherein the Ge atom is +4 oxidation state at original form, cleaves into HCl and $GeCl_2$ by hydrogen chloride elimination reaction. The cleaved molecule take place in the reaction as Ge(II) precursor, $GeCl_2$ to form stoichiometric GeTe through reaction with the Te precursor. This process was also combined with Sb_2Te_3 deposition process to obtain GeTe-Sb_2Te_3 pseubobinary films. Mechanism study on the deposition processes of binary GeTe and ternary GeSbTe films was performed.

Keywords: phase-change random access memory, atomic layer deposition, germanium telluride, germanium antimony telluride, deposition mechanisms

Student Number: 2011-22860

Taehong Gwon

Table of Contents

List of Figures

List of Abbreviations

DRAM	Dynamic random access memory
PCRAM	Phase-change random access memory
PCM	Phase-change material
V_{th}	Threshold voltage
NVM	Non-volatile memory
CVD	Chemical vapor deposition
ALD	Atomic layer deposition
XRF	X-ray fluorescence
GR	Growth rate
XPS	X-ray photoelectron spectroscopy
AES	Auger electron spectroscopy
XRD	X-ray diffraction
XRR	X-ray reflectivity
TEM	Transmission electron microscopy
FIB	Focused ion beam

1. Introduction

1.1. Atomic layer deposition process for phase-change random access memory

In the age of information, demands on memory devices increase which are faster, cheaper, and denser. The current semiconductor industry represented by dynamic random access memory (DRAM) and flash memory has grown along with the Moore's law of doubling density of memory every three years. However, as the size of DRAM and flash memory devices which has relatively complex and large structures is reduced to less than 20 nm, Moore's law is no longer sustainable. Moreover, due to the volatility of the DRAM and the high power operation, limited endurance, and slow operation speed of the flash memory device, there is a need for a new device that can overcome these problems. [1] Among these issues, newly proposed memory devices are called next-generation non-volatile memories. Phase-change random access memory (PCRAM) is one of next-generation non-volatile memories that records data on resistivity difference between amorphous and crystalline phase of phase-change materials (PCM). [2] PCRAM has high scalability due to its simple structure and can have higher density than DRAM in the same design rule. In addition, the operation speed of PCRAM is known to be several hundred times faster than that of NAND flash, and it also has much better endurance characteristics about

10^6~10^{12} than that of NAND flash, about 10^5. Based on these characteristics, PCRAM is expanding its market to replace NOR flash and apply it to storage class memory. For PCM, chalcogenide materials, which are known as materials containing group 16 elements, are widely used. Ternary materials consist with germanium, antimony, and tellurium, were widely studied as PCM which can also be used as materials for optical disks. Especially GeTe-Sb_2Te_3 pseudobinary materials showed feasibility for PCRAM application due to its phase stability, fast phase transformation speed. [3, 4]

However, there have been few studies on depositing materials of the composition through ALD manner. First, the complexity of ALD for multi-component materials is difficult challenge. [5] Multi-component ALDs are estimated to be much more complex than simple metal or metal oxide ALDs due to unpredictable chemical reactions involved by several precursors containing various elements. Second, $GeTe_2$ is deposited rather than GeTe due to the more stable property of the +4 oxidation state of Ge element. [6] It has been reported that obtained $GeTe_2$-Sb_2Te_3 pseudobinary composition can be degraded in operation characteristics ought to segregation of excess Te.

In this study, new chemical methods for binary GeTe films were suggested. To overcome aforementioned limitation, new pathways which forms different chemical species from original form of precursor were attempted, called intermediate precursor formation methods.

1.2. Objective and Chapter Overview

The objective of this dissertation is development of ALD process for binary GeTe or ternary GeSbTe films and its mechanism study.

Chapter 2 present the background studies needed for development of atomic layer deposition process of phase-changing materials.

Chapter 3 covers GeTe deposition process using $Ge(N(Si(CH_3)_3)_2)_2$ and $((CH_3)_3Si)_2Te$ as Ge- and Te-precursors. Combined process with previously settled Sb_2Te_3 for ternary GeSbTe was also performed.

Chapter 4 covers GeTe deposition process using $HGeCl_3$ and $((CH_3)_3Si)_2Te$ as Ge- and Te-precursors. Combined process with previously settled Sb_2Te_3 for ternary GeSbTe was also performed.

Chapter 5 covers lince-cell structured PCRAM device fabrication methods using E-beam lithography. Electrical properties of deposited GeTe film from chapter 3 and 4 was studied.

Finally, in chapter 6, the conclusion of the dissertation is made.

1.3. Bibliography

1. Jeong, D. S., Thomas, R., Katiyar, R. S., Scott, J. F., Kohlstedt, H., Petraru, A., and Hwang, C. S., *Reports on Progress in Physics* **75**, 31 (2012).
2. Raoux, S., Welnic, W., and Ielmini, D., *Chemical Reviews* **110**, 240-267 (2010).
3. Matsunaga, T., Morita, H., Kojima, R., Yamada, N., Kifune, K., Kubota, Y., Tabata, Y., Kim, J. J., Kobata, M., Ikenaga, E., and Kobayashi, K., *Journal of Applied Physics* **103**, (2008).
4. Matsunaga, T., and Yamada, N., *Physical Review B* **69**, (2004).
5. Lee, S. W., Choi, B. J., Eom, T., Han, J. H., Kim, S. K., Song, S. J., Lee, W., and Hwang, C. S., *Coordination Chemistry Reviews* **257**, 3154-3176 (2013).
6. Eom, T., Choi, S., Choi, B. J., Lee, M. H., Gwon, T., Rha, S. H., Lee, W., Kim, M. S., Xiao, M. C., Buchanan, I., Cho, D. Y., and Hwang, C. S., *Chemistry of Materials* **24**, 2099-2110 (2012).

2. Literature

2.1. Phase-change random access memory

As semiconductor devices represented by dynamic random access memory (DRAM) and NAND flash reached the scaling limit, new memories are emerging. [1] Of these emerging memories, Phase-change random access memory (PCRAM) is considered as the most mature technology. PCRAM is electrical memory using phase transition of chalcogenide materials. [2] This concept was started several tens of years ago from the optical disc using reflectance difference according to the crystallinity of chalcogenide materials, [3] and has now been applied to electronic devices technology.

Figure 2.1 shows a structure and operation scheme of typical PCRAM device. [4] PCRAM utilizes a large resistivity ratio between crystalline (low resistive state) and amorphous (high resistive state) of PCM. In order to reset the PCRAM device into amorphous phase, a large intensity of current pulse is applied to melt the programming region for a short time to be quenched right after melting. This process leaves high-resistivity amorphous material in the device. The amorphous region is electrically connected in series with the crystalline portion of the PCRAM which determines the resistance of the cell between top and bottom electrodes. In order to set the PCRAM cell in crystalline phase, moderate current pulse is applied for sufficient time enough to crystallize PCM in temperature range between crystallization temperature

and melting temperature. The measurement of the resistance of the cell is performed with current sufficiently small so as not to change the resistance state.

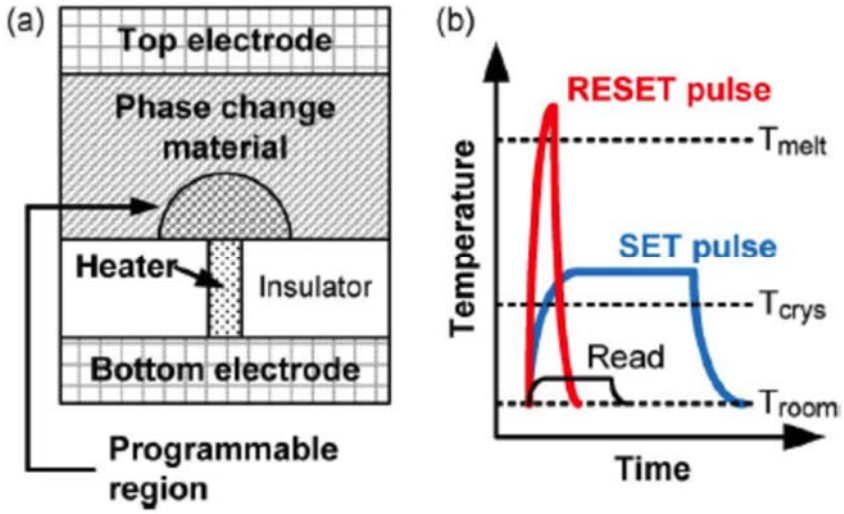

Figure 2-1 (a) Schematic diagram for cross-section of PCRAM device. (b) Electrical pulses for read/write/erase operations according to temperatures of the programmed region, respectively.

Figure 2-2 displays the current-voltage curves of the set and reset states. [5] Set and reset states have large resistance contrast at a voltage lower than threshold voltage (V_{th}). The reset state, which is high resistive state below the threshold state shows electrical threshold switching behavior at the V_{th}. This is a volatile resistivity changing phenomena that disappears when the voltage pulse is removed. However, when the voltage is applied sufficiently longer than the crystallization time, the memory switching phenomenon occurs and the device is changed into low resistance state. The set process is highly dependent of the mentioned threshold switching phenomenon. When the electric field applied to the amorphous region reaches the threshold value, the resistance of the amorphous region becomes low enough to be compared with the resistance of the crystalline state. Although the physical study of the phenomenon has not been completed yet, [6] it plays the main role in the phase-change operation at PCRAM device. The high resistive state of the PCRAM device requires very high energy to generate joule heat because the resistance is too high, however, the threshold switching greatly reduces the energy level required for the phase change which enable the set operation. The reset process consumes high electrical power because the PCM reaches to the melting point. The reset current is determined by various properties such as resistivity and thermal conductivity of the materials and device structure. In general, the operation speed of the PCRAM is determined by set operation speed due to longer time to completely crystallize the amorphous region.

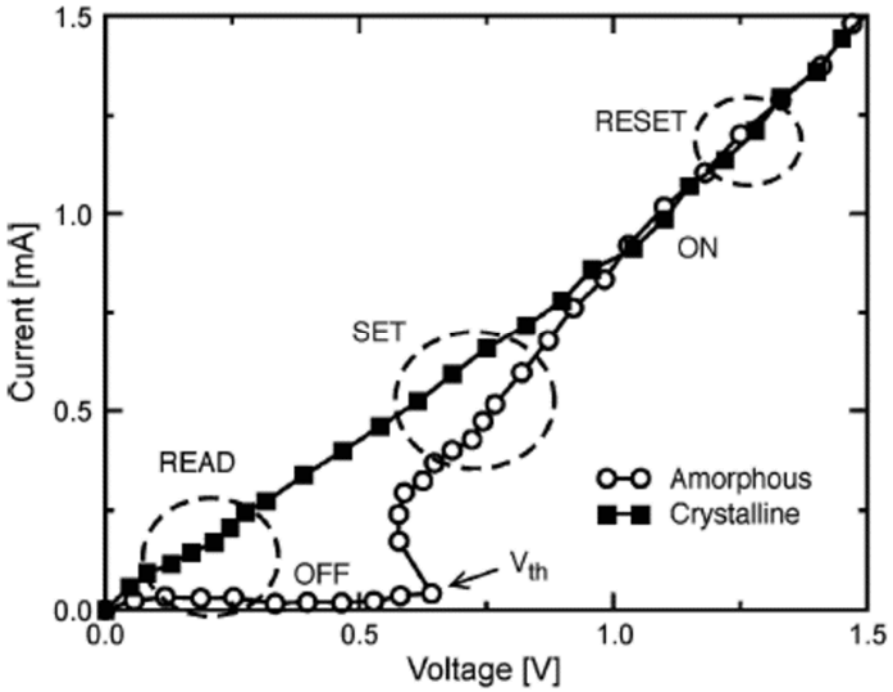

Figure 2-2 Current-voltage characteristics of set and reset states of PCRAM cell. The reset state shows threshold switching behavior.

As described above, the PCRAM device operation requires high reset current level. An attempt has been made to reduce the power consumption by improving the mushroom structure by increasing thermal efficiency. Figure 2-3 represents two ways for improvement. [7] Figure 2-3 (a) shows reducing the contact size to minimize working region, and Fig. 2-3 (b) displays minimizing through the structure of filling the PCM into a small hole. The confined structure described in Fig. 2-3 (b) has become new standards for PCRAM due to many profits in the fabrication process of the PCRAM such as higher thermal efficiency, improved cross-talk issue among neighborhood cells, and strong resistance against etching damage. [8]

.

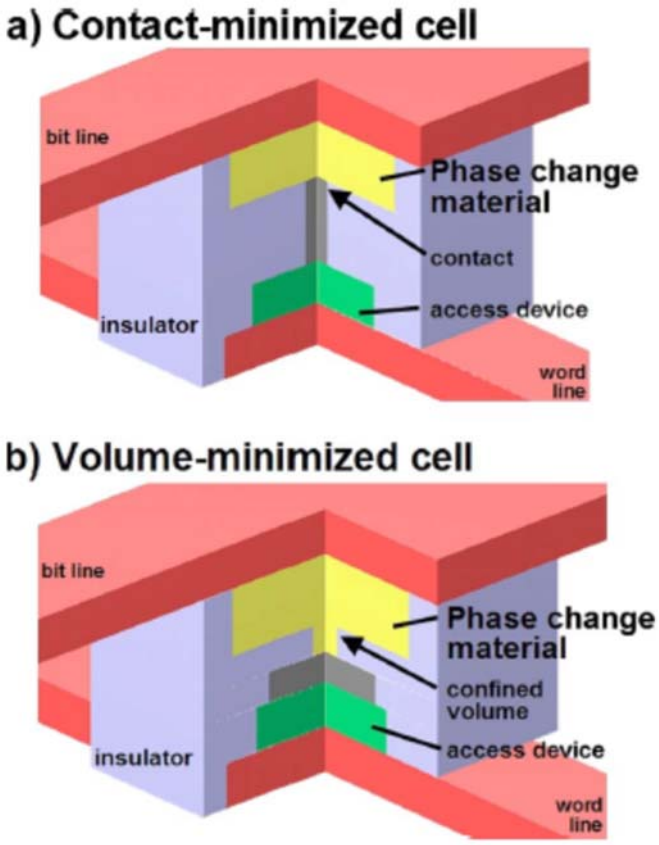

Figure 2-3 Types for phase-change memory device : (a) contact-minimized cell and (b) volume-minimized cell.

2.2. Atomic layer deposition

Atomic layer deposition is emerging as an important technology for depositing thin films in various applications. [9] Semiconductor processing has been one of the main objectives of recent ALD development. As the semiconductor industry move towards high level of scaling, atomic level controlling of the film was required. The miniaturization required the property of conformal coating on very high aspect ratio structures. The conformality obtained through ALD in the high aspect ratio structure was much better than that of other deposition technique. The needs for a process forming a void-free films in semiconductor devices has been the basis for the development of ALD technology. ALD can control atomic layers and conformally deposit using sequential, self-limiting surface reactions. Figure 2-4 shows a schematic diagram of this behavior. [10] A typical ALD process is based on two reaction sequences consist with two surface reactions. Only a limited amount of thin film grows because the number of sites able to react is limited. If the two surface reactions are self-limiting, respectively, the process can progress sequentially and adjust film to the atomic level of thickness. Figure 2-5 displays actual result for cross-sectional SEM image of an Al_2O_3 ALD film with a thickness of 300 nm on a trench structured Si wafer. [11]

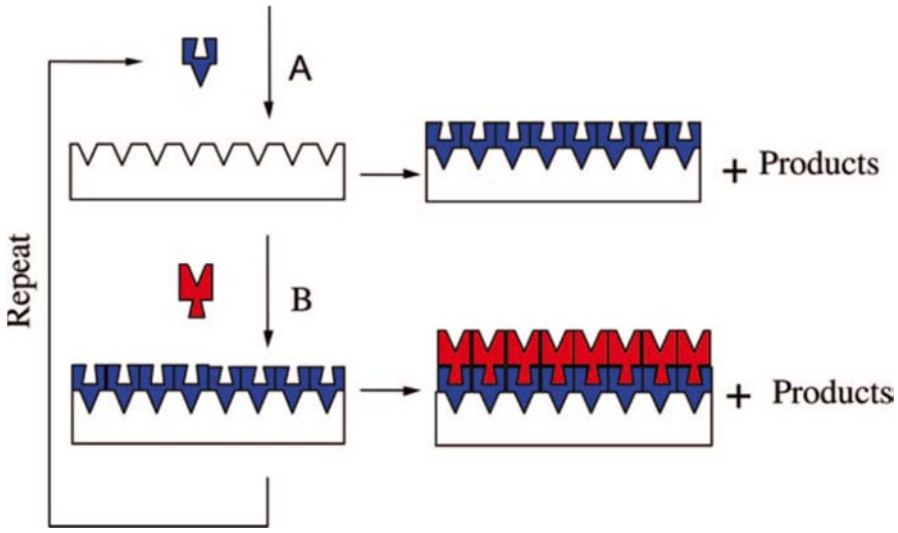

Figure 2-4 Schematic representation of ALD process using self-limiting behavior for AB binary reaction sequence.

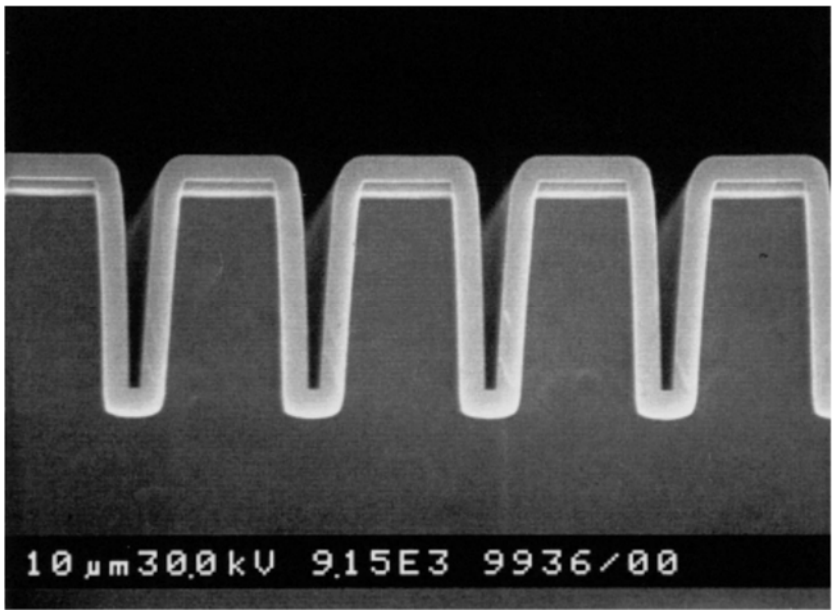

Figure 2-5 Cross-sectional SEM image for Al_2O_3 films deposited on trench structured Si wafer by ALD

The ideal ALD model, represented by Al2O3 deposition, may not be applied in other ALD systems. Some ALD systems may be adsorbed more as the precursor decomposes at the surface which cause no self-limiting reactions. In other ALD systems, some precursors may have surface reactions not fully reactive. This reaction can leave a lot of impurities in the film even though it exhibits self-limiting reaction. The temperature range, referred as “ALD window” is an area which shows nearly ideal ALD behavior existing between temperatures of non-ideal behaviors, as shown in Fig. 2-6. At low temperatures, the reactants may condense on the surface. Or, the thermal energy required for the surface reaction may be insufficient. And at high temperatures, the precursor may be thermally decomposed or desorbed rather than ideal ALD behaviors.

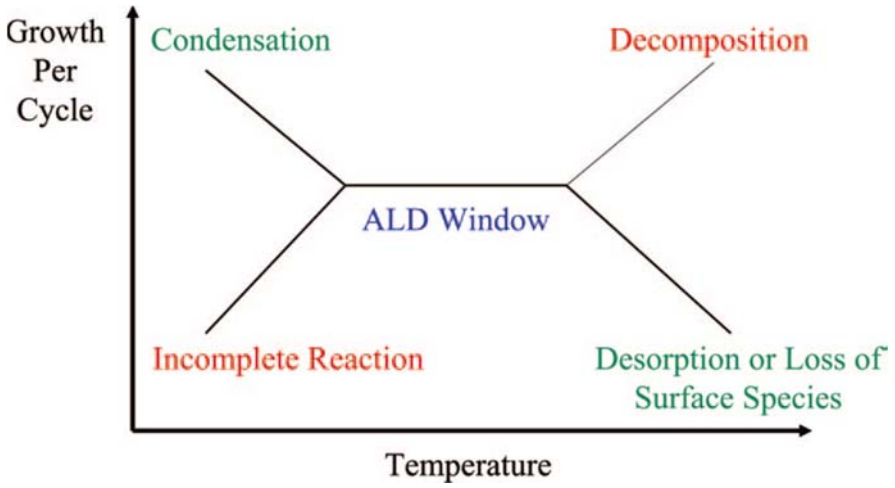

Figure 2-6 Schematic ALD behavior of growth rate for temperature ranges showing “ALD window”

2.3. Bibliography

1. Jeong, D. S., Thomas, R., Katiyar, R. S., Scott, J. F., Kohlstedt, H., Petraru, A., and Hwang, C. S., *Reports on Progress in Physics* **75**, 31 (2012).
2. Raoux, S., Welnic, W., and Ielmini, D., *Chemical Reviews* **110**, 240 -267 (2010).
3. Chen, M., Rubin, K. A., and Barton, R. W., *Applied Physics Letter s* **49**, 502-504 (1986).
4. Wong, H. S. P., Raoux, S., Kim, S., Liang, J. L., Reifenberg, J. P., Rajendran, B., Asheghi, M., and Goodson, K. E., *Proceedings of t he Ieee* **98**, 2201-2227 (2010).
5. Pirovano, A., Lacaita, A. L., Pellizzer, F., Kostylev, S. A., Benvenu ti, A., and Bez, R., *Ieee Transactions on Electron Devices* **51**, 714-719 (2004).
6. Adler, D., Shur, M. S., Silver, M., and Ovshinsky, S. R., *Journal o f Applied Physics* **51**, 3289-3309 (1980).
7. Raoux, S., Burr, G. W., Breitwisch, M. J., Rettner, C. T., Chen, Y. C., Shelby, R. M., Salinga, M., Krebs, D., Chen, S. H., Lung, H. L., and Lam, C. H., *Ibm Journal of Research and Development* **52**, 465-479 (2008).
8. Cho, S. L., Yi, J. H., Ha, Y. H., Kuh, B. J., Lee, C. M., Park, J. H., Nam, S. D., Horii, H., Cho, B. K., Ryoo, K. C., Park, S. O.,

Kim, H. S., Chung, U.-i., Moon, J. T., and Ryu, B.-I. In *Highly S calable on-Axis Confined Cell Structure for High Density Pram Bey ond 256mb*, Symposium on VLSI Technology 2005, 2005; IEEE.

9. George, S. M., *Chemical Reviews* **110**, 111-131 (2010).
10. George, S. M., Ott, A. W., and Klaus, J. W., *Journal of Physical Chemistry* **100**, 13121-13131 (1996).
11. Ritala, M., Leskela, M., Dekker, J. P., Mutsaers, C., Soininen, P. J., and Skarp, J., *Chemical Vapor Deposition* **5**, 7-9 (1999).
12. Suntola, T. Atomic Layer Epitaxy. In *Handbook of Crystal Growth, Vol. 3, Part B: Growth Mechanisms and Dynamics*; Hurle, D. T. J., Ed.; Elsevier: Amsterdam, 1994; Chapter 14.

3. Atomic layer deposition of GeTe films using $Ge\{N[Si(CH_3)_3]_2\}_2$, $\{(CH_3)_3Si\}_2Te$, and methanol

3.1. Introduction

Recent innovations in information technology require non-volatile memory (NVM) with higher density, faster operation speed, and lower power consumption. Phase-change random access memory (PCRAM), which records data through the resistance difference between amorphous and crystalline phases of the phase change material (PCM), is one of the strongest candidates in NVM for its fast operation speed, stable retention property and good scalability. Although many kinds of materials have been researched, the most widely used PCMs are ternary GeSbTe materials, especially alloys whose composition lies on the GeTe-Sb_2Te_3 pseudo-binary tie line.[1, 2] Among the compositions on the tie line, GeTe-richer materials have better data retention properties, and Sb_2Te_3-richer materials have faster phase change characteristics.[3, 4] Among the various compositions, $Ge_2Sb_2Te_5$ (called GST225) has become the base material in PCRAM application.

In the early stage, PCRAM devices had a mushroom structure constructed with planar PCM and a small bottom electrode contact. This structure has

limitation for scaling because of its low thermal efficiency and thermal cross-talk issues.[5] To overcome these problems, a new device structure, called confined cell structure, where PCM is plugged into a small contact hole, was suggested.[6] However, to fabricate a confined cell structure, PCM should be deposited with high conformality which could be achieved by either chemical vapor deposition (CVD) or atomic layer deposition (ALD) possess.

There have been several reports on the CVD of GeSbTe films using precursors which have alkyl- or amino- ligands with reducing gases and plasma power.[7-11] However, adoption of plasma to activate chemical reactivity of the precursors resulted in poor conformality. Meanwhile, results of ALD-type deposition of GeSbTe were not promising because of low reactivity of the alkyl- or amino-based precursors due to their high chemical stability. Recently, Pore et al. reported the ALD of binary GeTe, Sb_2Te_3 and ternary $Ge_2Sb_2Te_5$ using chlorine-based Ge- and Sb-precursors and silyl-based Te-precursor,[12-14] which triggered active research on ALD of GeSbTe films by the authors‘ group using similar chemical reactions but with slightly different precursors.[15, 16] The authors reported ALD of films with compositions lying on $GeTe_2$-Sb_2Te_3 pseudo-binary tie line using precursors; $Ge(OCH_3)_4$, $Sb(OC_2H_5)_3$, and $((CH_3)_3Si)_2Te$.[15, 16] While there were several promising aspects from this chemistry-specific ALD process, it also showed a limitation in controlling film composition. As mentioned above, the most widely used material in PCRAM application is $Ge_2Sb_2Te_5$ but it cannot be deposited by this method due to the

formation of $GeTe_2$ rather than GeTe. GeTe or $GeTe_2$ itself can hardly be a feasible phase change memory material, but is still constitute the critical component of more feasible Ge-Sb-Te (or even doped materials) compounds. Therefore, detailed study on the ALD behavior of GeTe is important. Ge atoms in the Ge-precursor are in the +4 oxidation state (tetravalent Ge precursor), and when these perform ligand exchange reactions with the Te-precursor, where Te has -2 oxidation state, a composition with a ratio of Ge:Te = 1:2 is formed. To solve this problem, a divalent Ge-precursor wherein the Ge atom has +2 oxidation state is necessary. However, the natural preference of Ge atoms toward the +4 oxidation state hinders development of such precursors. In the reports on CVD or ALD for materials containing Ge, most of the Ge-precursors are tetravalent precursors.[7-11, 15, 17, 18] There are several divalent Ge-precursors, but most of them make ring or polymeric-chain involving Ge-Ge bond which is not optimum for ALD process. Adding adducts or adopting bulkier ligands to stabilize monomeric divalent Ge-precursors has been reported to be a feasible approach to stabilize monomeric configuration of divalent Ge-precursors.[14, 19-21] In this report, a monomeric and stable Ge-precursor, $Ge(N(Si(CH_3)_3)_2)_2$, which is divalent and is stabilized by the bulkiness of the $N(Si(CH_3)_3)_2$ ligands, is adopted to deposit the GeTe films in ALD manner with $((CH_3)_3Si)_2Te$ as the Te-precursor. The Ge precursor has become promising Ge ALD precursor with reactivity to hydrogen or ammonia gas,[22] and also used to make nanoparticle in liquid phase.[23-25] However, as the results will show, there was almost no

ALD-type chemical reaction between these two precursors, which is probably due to the blocking effect of the two bulky substituents of this Ge-precursor. The reaction byproduct $((CH_3)_3Si)_3N$ is kinetically unstable compound, even though the Te-precursor has shown a high reactivity toward the chloride and alkoxide forms of Ge-precursors.[12-16] Therefore, an alternative reaction route utilizing high chemical activity of methanol toward the Ge- and Te-precursors was explored in this study. It was found that complicated chemical reaction routes exist involving several intermediates, which enabled deposition of GeTe films in ALD-specific saturation manner.

3.2. Experimental Procedures

GeTe films were deposited using a shower-head-type ALD reactor with a 6-inch-wafer scale (CN-1, Atomic-premium). The substrate temperature was maintained at 70 °C except for test results of temperature effect. The precursors of Ge and Te were $Ge(N(Si(CH_3)_3)_2)_2$ and $((CH_3)_3Si)_2Te$, respectively. Each precursor was contained in separated stainless steel canisters. For the Ge-precursor, the canister was maintained two different conditions, at 50 or 70°C to control injection rate of the precursor, and for Te-precursor, the canister was at 35°C. The vapor pressures of $Ge(N(Si(CH_3)_3)_2)_2$ are 0.05 [0.2] at 50 [70] °C, whereas that of $((CH_3)_3Si)_2Te$ at 35 °C is 1 Torr. The vapors of Ge- and Te-precursors were carried into the reactor by 100, 50 standard cubic centimeters per minute (sccm) of Ar gas, respectively. Thermally evaporated methanol vapor at room temperature was injected into the reactor with the help of 200 sccm of Ar carrier gas. Because of its high vapor pressure, methanol injection rate was controlled using metering valve. Each precursors and methanol vapor are injected through gas line made by stainless steel, and the gas flow line was maintained 100 °C except for test results of shared gas line temperature, which is higher enough than canister temperature to avoid condensation of the evaporated precursor molecules. 200 sccm of Ar gas was used to purge out excess precursor and byproducts after precursor injection sequence. The chamber has pumping system with dry-pump (QDP80, Edwards), and its base

pressure and working pressure is 30 mTorr and 1-2.5 Torr, respectively. The process recipes were constructed to induce reaction among precursors, methanol vapor, and their intermediates. In 50 °C Ge-precursor condition, for the deposition of GeTe films, 100 super cycle of precursor sequence as follows was used as the base-line process recipe: methanol pulse (3 s) – Ge-precursor/methanol pulse (5 s) – methanol pulse (5 s) – Ge purge (10 s) – methanol pulse (3 s) – Te-precursor/methanol pulse (2 s) – Te purge (5 s), otherwise specified to check ALD type self-limiting behavior. Modified sequences with different methanol injection conditions were also tested to check the role of methanol in the process. In 70 °C Ge-precursor condition, similarly, 100 super cycle of base-line precursor sequence as follows was used: methanol pulse (3 s) – Ge-precursor/methanol pulse (15 s) – methanol pulse (5 s) – Ge purge (10 s) – methanol pulse (3 s) – Te-precursor/methanol pulse (2 s) – Te purge (5 s).

SiO_2/Si and TiN/Ti/SiO_2/Si wafer were used as substrates which have thermally grown 100-nm-thick SiO_2 film, sputtered 50-nm-thick TiN film and 5-nm-thick Ti film (called SiO_2 and TiN substrate, respectively). The layer densities of the films were measured by X-ray fluorescence spectroscopy (XRF, Thermo Scientific, Quant'X EDXRF), and the growth rate (GR) was calculated by dividing the layer density by supercycle number. X-ray photoelectron spectroscopy(XPS) was used to check chemical state of elements in film and performed at 4D beamline in Pohang Light Source. The impurity level was

checked by Auger Electron Spectroscopy (AES, Perkin-Elmer, PHI 660). The crystallinity and density of films was measured by X-ray diffraction (XRD) and X-ray reflectivity (XRR) using X-ray diffractometer (PANalytical, X'Pert PRO MPD). The film thickness was calculated by dividing layer density measured by XRF by the density of each film measured by XRR. Step coverage of film deposited on hole structure was estimated by transmission electron microscopy (TEM, Tecnai, F20) using specimen prepared by focused ion beam (FIB, FEI, Helios 650).

3.3. Results and Discussions

First, the chemical reactivity between the Ge- and Te-precursors were tested using a typical ALD sequence shown in Fig. 3-1 (a) (called Ge-Te sequence), with no methanol step. The GR was compared with a previously reported Sb_2Te_3 ALD process[15] using the same Te precursor but with $Sb(OC_2H_5)_3$ as Sb-precursor (called Sb-Te sequence). The process with respective Ge, Sb, and Te precursors pulse/purge times of 5 s/ 5 s, 3 s/ 60 s, and 2 s/ 60 s were used. As can be seen in Fig. 3-1 (b), almost no growth of GeTe film was observed (red circle symbol). This means that the simplest ligand exchange reaction between the two precursors represented Equation 3.1 does not occur. On the other hand, the Sb-Te sequence resulted in formation of a Sb_2Te_3 film (black square symbol) which is consistent with the previous report.[15]

$$Ge(N(Si(CH_3)_3)_2)_2 + ((CH_3)_3Si)_2Te \rightarrow \quad GeTe + N(Si(CH_3)_3)_3$$

Equation 3.1

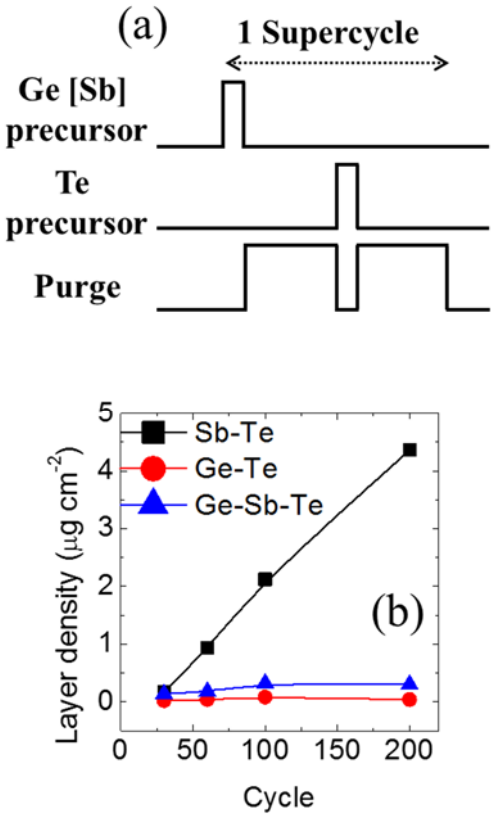

Figure 3-1 (a) Schematic diagram for Ge[Sb]–Te sequence (without methanol). (b) Comparison of growth behavior using Ge-Te, Sb-Te and Ge-Sb-Te sequences where Ge-Sb-Te sequence is the combined sequence with Ge-Te and Sb-Te sequences.

However, combining the Ge-Te sequence with the Sb-Te sequence (called Ge-Sb-Te sequence) resulted not only in no GeTe film growth but also a large decrease in the growth rate of Sb_2Te_3 (blue triangle symbol), even though the Ge-Sb-Te sequence contained an identical number of subcycles of Sb-Te. This suggests that the Ge-precursor has a strong surface passivation effect which inhibits chemical adsorption of other precursors during their subsequent pulse steps. Even if the Ge precursor is able to adsorb to the substrate, low reactivity and bulky nature of $N(Si(CH_3)_3)_2$ ligands suppresses further chemical adsorption of other precursors on top of chemisorbed $Ge(N(Si(CH_3)_3)_2)_2$ molecules. Therefore, the $Ge(N(Si(CH_3)_3)_2)_2$ was not a suitable Ge-precursor if no further modification of the reaction route is provided, although it is a divalent Ge-precursor.

To mitigate the passivation effect and to enhance the reactivity of the Ge-precursor, methanol vapor was co-injected to form intermediate Ge-precursor in the gas phase. It was speculated that an intermediate reaction product $Ge(OCH_3)_2$, which contains divalent Ge but is not a stable compound, could be formed within the gas phase of the ALD chamber or on the surface of the substrate according to the following Equation 3.2. It is proposed that $Ge(OCH_3)_2$ reacts with $((CH_3)_3Si)_2Te$ to form GeTe. It was also confirmed that repeated co-injection of $Ge(N(Si(CH_3)_3)_2)_2$ and methanol did not induce any film formation suggesting that thermal decomposition of $Ge(N(Si(CH_3)_3)_2)_2$ and $Ge(OCH_3)_2$ is not of concern.

$$Ge(N(Si(CH_3)_3)_2)_2 + 6CH_3OH \rightarrow Ge(OCH_3)_2 + 2NH_3 + 4CH_3OSi(CH_3)_3$$

Equation 3.2

Several pre-tests were performed to maximize the efficiency of reactions represented Equation 3.2. First, the methanol and precursors were separately introduced into the chamber, anticipating an ALD-like reaction wherein adsorption of $Ge(N(Si(CH_3)_3)_2)_2$ on film surface is followed by reaction with methanol on the film surface. However, this did not work very well, possibly due to low efficiency of such surface reaction or the surface passivation effects of the remaining $Ge(N(Si(CH_3)_3)_2)_2$. Therefore, it was necessary to co-inject the methanol and $Ge(N(Si(CH_3)_3)_2)_2$ to induce sufficient ALD reaction. It was also found that injecting methanol alone, both before and after the co-injection of methanol and $Ge(N(Si(CH_3)_3)_2)_2$ was necessary for reproducible film growth. This is believed to be due to excess $Ge(N(Si(CH_3)_3)_2)_2$ molecules on the chamber wall which might not be sufficiently purged out during the subsequent purge step. Injecting methanol alone sufficiently removed the remaining $Ge(N(Si(CH_3)_3)_2)_2$, and process reproducibility was confirmed. Therefore, an optimized ALD sequence could be setup as shown in Fig. 3-2 (a), where methanol-only injections were added before (for 3 s) and after (for 5 s) the co-injection of methanol and $Ge(N(Si(CH_3)_3)_2)_2$.

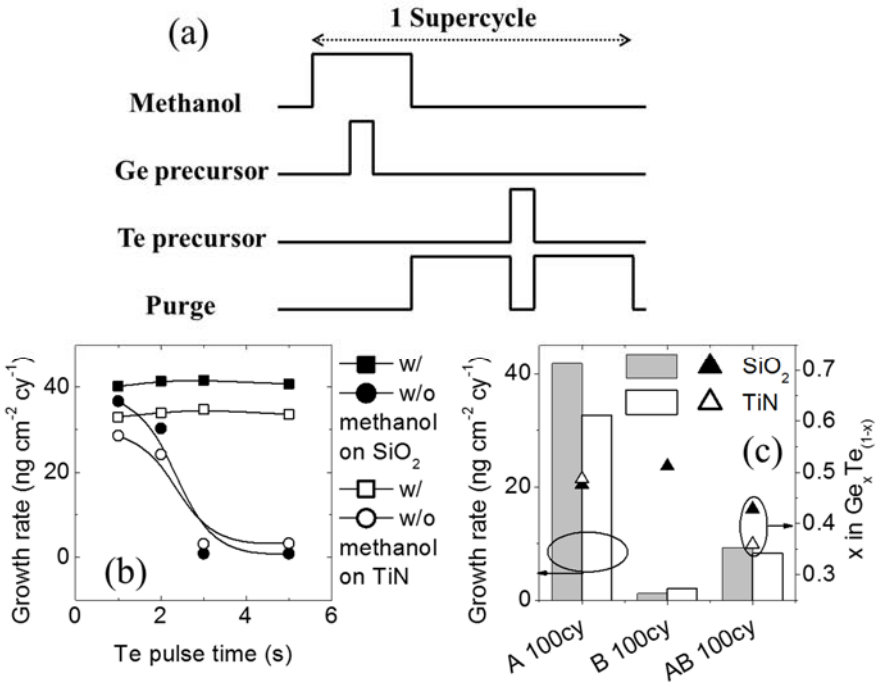

Figure 3-2 (a) Schematic diagram for sequence where the Ge-precursor co-injected with methanol. The Te-precursor was injected without methanol. (b) Comparison between growth behaviors using different Te-precursor injection conditions; with methanol and without methanol on SiO_2 and TiN substrates. (c) Comparison between processes using different sequences on SiO_2 and TiN substrates. Sequence A where the Ge- and Te-precursors were co-injected with methanol, B where only Ge-precursor was co-injected with methanol (with 5 s-long Te-precursor pulse), and AB where sequence A and B were conducted alternately.

Under this ALD condition, the intermediate Ge-precursors formed by the Equation 3.2 is expected to react well with the Te precursor to form GeTe film by the following Equation 3.3Equation 3.3

$$Ge(OCH_3)_2 + ((CH_3)_3Si)_2Te \rightarrow GeTe + 2(CH_3)_3SiOCH_3$$

Equation 3.3

However, generating (intermediate) Ge-precursors having +2 oxidation state of Ge does not necessarily guarantee the deposition of stoichiometric GeTe film, but there were certain experimental conditions that could result in predominantly GeTe as discussed later.

Figure 3-2 (b) shows the variation in the GR as a function of Te-precursor injection time (t_{inj}), where the Te injection was made simultaneously with methanol (square symbol) or without methanol (circle symbol). When only the Te-precursor was injected GR degraded significantly with increasing t_{inj} while this was not the case when methanol was co-injected. This suggests that pristine $((CH_3)_3Si)_2Te$ molecules also induce a surface passivation effect on the $Ge(OCH_3)_2$ pulsed surface, details of which are unclear at this moment, although it has shown high reactivity toward other Ge- and Sb-precursors.[15, 16] This revealed that the actual reactions to deposit GeTe cannot be represented

by Equation 3.3. More probable reaction pathways are discussed below using Equation 3.4 and Equation 3.5, where the formation of a more efficient intermediate precursor H_2Te as the actual reactant molecule is suggested. The high GR for the short t_{inj} without methanol could be understood from the influence of remaining methanol even after the previous purge step. To further confirm the influence of methanol during the Te-precursor injection step, the following experiments were performed, of which results are shown in Fig. 3-2 (c). Here, sequence A means that methanol was co-injected with both the Ge- and Te-precursors, while sequence B means that methanol was co-injected with the Ge-precursor only. AB means the alternative adoption of A and B sequences. Total cycle number was fixed at 100, and the precursor injection time was 5 s / 2 s for sequence A, and 5 s/ 5 s for sequence B, respectively. While sequence A resulted in film growth with film composition close to GeTe stoichiometry, sequence B resulted in almost no film growth, which could be understood from the passivation effect of $((CH_3)_3Si)_2Te$. Interestingly, sequence AB resulted in a film growth lower than half that of sequence A, suggesting that the sequence B adversely interfered with the film growth by sequence A. Because methanol was co-injected only with Ge-precursor in sequence B, the adverse effect must originate from the pristine Te-precursor. Adsorption of this precursor on the film surface seemed to decrease the density of active sites available for adsorption of the intermediate Ge-precursor. This is consistent with the

conjecture that pristine Te-precursor does not react with the intermediate Ge-precursor in Fig. 3-2 (b).

The reaction between the Te-precursor and methanol may result in the in-situ generation of H_2Te as a transient intermediate species according to the following Equation 3.4, and the H_2Te may react with the intermediate Ge-precursor to form GeTe films according to Equation 3.5;

$$((CH_3)_3Si)_2Te + 2CH_3OH \rightarrow H_2Te + 2CH_3OSi(CH_3)_3$$

Equation 3.4

$$H_2Te + Ge(OCH_3)_2 \rightarrow GeTe + 2CH_3OH$$

Equation 3.5

Therefore, it was turned out that the actual (ideal) ALD reaction for depositing GeTe could be represented by Equation 3.5 which represents the ALD reaction between the two intermediate precursors, although additional reaction interferes to make the process more complex as can be seen later.

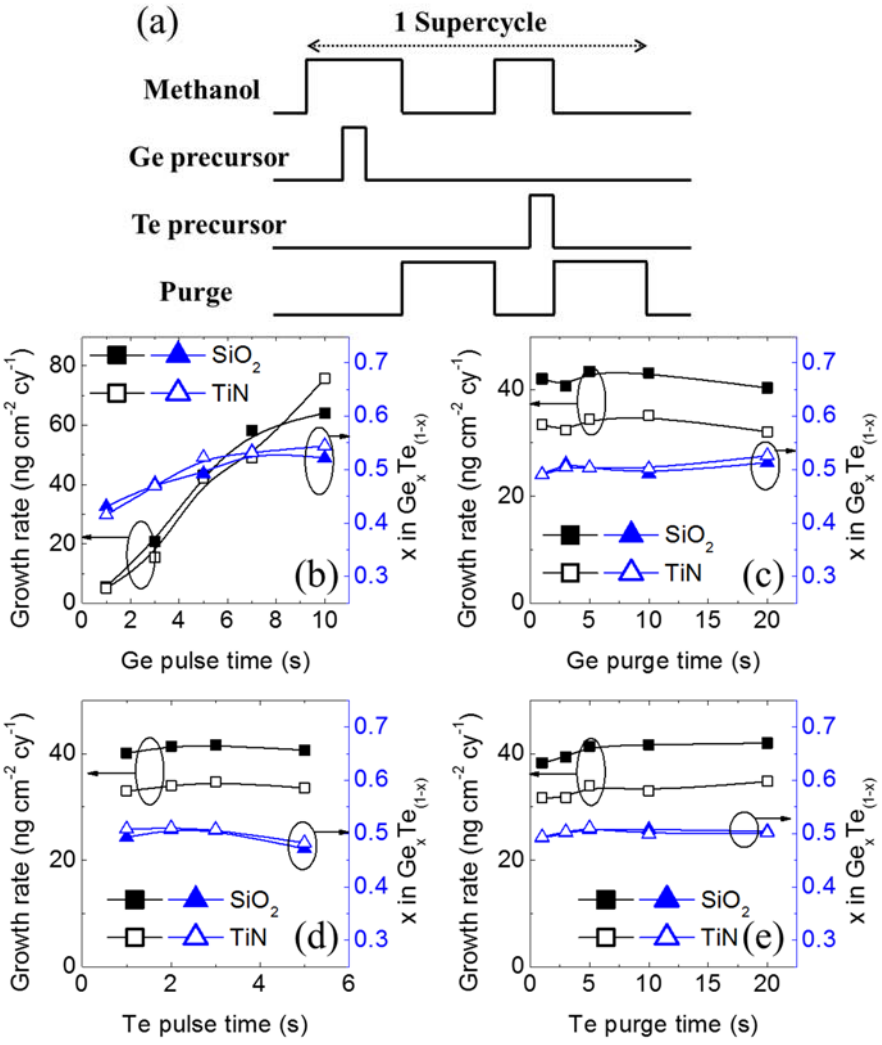

Figure 3-3 (a) Schematic diagram for base-line sequence for GeTe deposition. (b) – (e) Variations in growth rate and composition as a function of the precursor pulse and purge times. Black square and blue triangle symbols indicate the growth rate and x in $Ge_xTe_{(1-x)}$, respectively.

As a result of all these preliminary experiments, it was concluded that both the Ge- and Te-precursors should be co-injected with methanol in order to form the reactive intermediates for the ALD-type deposition process. Process control was improved by additional injection of methanol both before and after the Ge-precursor and methanol injection step. This allows for complete conversion of the passivating $Ge(N(Si(CH_3)_3)_2)_2$ to the reactive intermediate during the entire ALD process. In contrast, additional methanol injection was only necessary before, but not after, the Te-precursor and methanol injection step. This is perhaps due to the faster reaction rate of $((CH_3)_3Si)_2Te$ with methanol or faster removal of unreacted $((CH_3)_3Si)_2Te$ during the purge step. The ALD sequence established for growth of a GeTe film is represented by Fig. 3-3 (a), wherein the Ge-precursor is co-injected during the middle part of a relatively long methanol injection step, and the Te-precursor is co-injected at the end of a somewhat shorter methanol injections step. Although direct use of H_2Te might be considered as an alternative to the co-injection of $((CH_3)_3Si)_2Te$ and methanol, it would be difficult to use because of its low stability and high toxicity.[26] Under these experimental conditions, the film composition appears to be saturated at a x value ~0.52 with sufficiently long Ge injection time which is slightly deviated from the expected value according to Equation 3.5. The more significant problem is that the growth rate did not saturate even at a prolonged injection time of 10 s, suggesting that the saturated ALD reaction has not been attained even under this condition. This problem will be dealt with in

much more detail later. Figures 3-3 (b) – (e) show the growth behavior of GeTe layers as a function of t_{inj} and purge time (t_{prg}) of Ge- and Te-precursors, respectively, on SiO_2 (filled symbol) and TiN (open symbol) substrates. In Fig. 3-3 (b), the change in film composition can be observed with varying t_{inj} of the Ge-precursor, which suggests that reactions other than in Equation 3.5 also can occur. The desired 1:1 composition can be obtained at 5 s of t_{inj} for Ge-precursor through modulating t_{prg} of Ge- and Te-precursors and t_{inj} of Te-precursor. By comparing Figs. 3-3 (b) and (d), it is reasonable to assume that different Ge intermediate precursors exist in addition to $Ge(OMe)_2$ produced by Equation 3.2. The following experiments provided detailed models for the intervening chemical reactions.

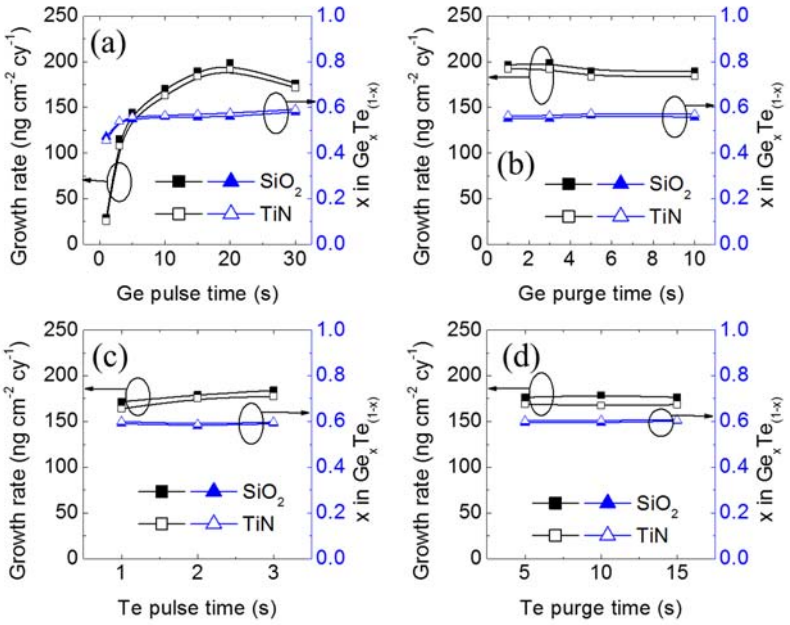

Figure 3-4 (a) - (d) Results of the repeated experiment in Fig. 3-3 at an elevated Ge-precursor temperature of 70 °C. Saturation behaviors in both growth rate and composition were observed.

It should be noted again that the co-injection of both Ge- precursor and methanol does not make a film since the reaction must be terminated by the ligand exchange between intermediate Ge- and Te-precursors. Therefore, using longer t_{inj} for Ge-precursor or higher Ge-precursor injection rate, large quantity of intermediate precursors is expected to be steadily present inside the ALD chamber or surface of the growing film. In addition, the non-saturating growth rate with t_{inj} of Ge-precursor in Fig. 3-3 (a) could be ascribed to the still insufficient precursor injection despite the long t_{inj}. To verify this behavior, the experiments in Fig. 3-3 were repeated with canister temperature of the Ge-precursor raised to 70 °C for higher injection rate, where its vapor pressure is four-times higher, of which the result is summarized in Fig. 3-4. Figure 3-4 (a) displays the growth rate and composition of $Ge_xTe_{(1-x)}$ in which saturation behavior can be clearly observed due to higher injection rate of the Ge-precursor. Figures 3-4 (b) - (d) also showed consistent saturated growth rate and composition with other injection and purge conditions, indicating ideal ALD condition. The saturation level of the growth rate was ~four times higher compared with the results in Fig. 3-3, being consistent with the four times higher vapor pressure of the Ge-precursor under this condition. The slightly decreased growth rate at the t_{inj} of 30 s in Fig. 3-4 (a) might be related with the depletion of precursor molecules within the Ge-canister volume under such excessively long t_{inj}. Under this circumstance, the carrier gas, being deleted of precursor, actually purges out the surface adsorbed by molecules and growth

rate slightly decreases. These results indicate that the genuine ALD-type growth behavior can be achieved under these modified growth conditions. Nevertheless, the saturated film composition, x ~ 0.6 ($Ge_{0.6}Te_{0.4}$), was quite extraordinary from the material chemistry point of view; this composition suggests that the overall oxidation state of Ge is < +2 or contains some concentration of zero-valent Ge atoms within the film. Therefore, this composition requires careful reconsideration of suggested ALD reaction mechanism so far, and it is necessary to invoke additional reaction routes that may result in the Ge-Ge bonds. Therefore, the tentative reaction pathways were suggested as shown in Fig. 3-5. It should be mentioned that the reaction mechanisms displayed in Fig. 3-5 are not experimentally proven by a rigorous chemical analysis but based on the general knowledge in the field. This analysis is based on the possible formation of various Ge-intermediates such as germylene.

(a)

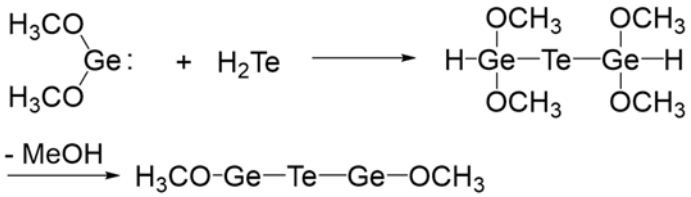

(b)

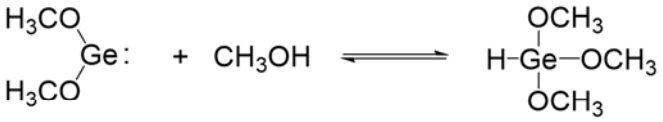

(c)

(d)

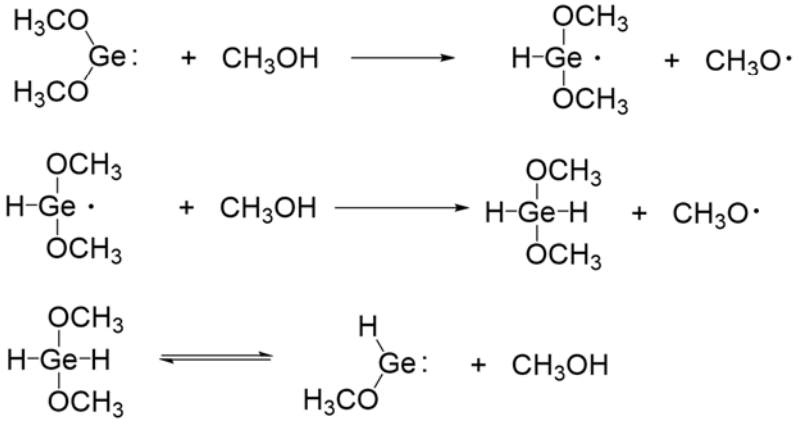

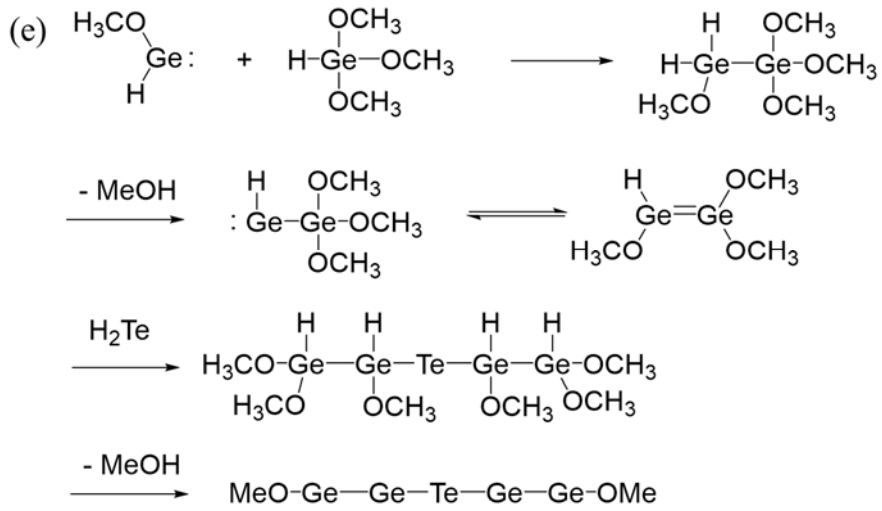

Figure 3-5 (a) – (c) Models of schematic mechanism for additional reaction between intermediate Ge-precursors and methanol (d), (e) Schematic diagram for deposition by reaction among produced intermediate Ge- and Te-precursors to make stoichiometric GeTe or Ge-richer film formation, respectively.

Figure 3-5 illustrates possible chemical reaction schemes between $Ge(OMe)_2$ and rich atmosphere of methanol vapor to form $HGe(OMe)_3$, $Ge(OMe)_4$, HGeOMe, and even more complicated species. The composition of the film is determined based on the number of exchangeable ligand that is available in Ge-precursor. Figure 3-5 (a) indicates a more detailed mechanism, which was originally intended for this work and explained by the aforementioned Equation 3.5. However, it is also probable that the $Ge(OCH_3)_2$ reacts further with another CH_3OH molecule to form $HGe(OCH_3)_3$ (trimethoxygermane) according to Fig. 3-5 (b). However, the oxidation state of Ge atom in this intermediate molecule should most likely be +2, so it may also form GeTe when it reacts with H_2Te afterwards. There is yet another possibility that this HGe($OCH_3$3 molecule reacts with CH_3OH molecule again to form $Ge(OCH_3)_4$ (tetramethoxygermane) which most likely forms the unwanted $GeTe_2$.[15]

However, none of these suggested reaction can explain the experimental results showing the $Ge_{0.6}Te_{0.4}$ film formation. This implies that there must be certain mechanism(s) that can result in the Ge-Ge bond in the film. As will be shown later by XPS using synchrotron X-ray source, the Ge-rich film (x ~0.6) indeed has Ge-Ge bonds. For such mechanism, the reaction routes described in Figs. 3-5 (d) and (e) are considered. According to the two-step process indicated by the upper two reaction schemes in Fig. 3-5 (d), $H_2Ge(OCH_3)_2$ (dimethoxygermane) intermediate molecules might be formed. This new intermediated species can be further decomposed to $HGe(OCH_3)$

(monomethoxygermylene) and methanol as shown by the last reaction scheme in Fig. 3-5 (d). $HGe(OCH_3)$ must be quite unstable because the small size of H and OCH_3 ligands cannot fully stabilize the central electron lone pair. So, they may react with several other intermediates in the chamber or film surface, and among them, the reaction pathway that can induce the Ge-Ge bond is summarized in Fig. 3-5 (e). In this case, monomethoxygermylene reacts with $HGe(OCH_3)_3$ molecule and ended up with $H(OCH_3)Ge=Ge(OCH_3)_2$ as shown by the second row of Fig. 3-5 (e). Then, these complicated molecules can react with H_2Te according to the third row and lose methanol subsequently, which most likely results in the molecular structure containing the Ge-Ge-Te-Ge-Ge bonding configuration as shown by the last row of Fig. 3-5 (e). These reaction sequences, although it is rather complicated, can thoroughly explain the Ge-Ge bond formation during the ALD. If only this type of reaction contributed to the film growth, the film composition must be Ge_2Te. Therefore, the experimental film composition of $Ge_{0.6}Te_{0.4}$ can be obtained when the GeTe and Ge_2Te formations occur with a ratio of 1:1, suggesting that Ge-intermediates with Ge^{2+}, such as $Ge(OCH_3)_2$, $HGe(OCH_3)_3$, and with Ge=Ge bond, such as $H(OCH_3)Ge=Ge(OCH_3)_2$, have an almost equal probablity of formations. It is also noted that the formation of $H(OCH_3)Ge=Ge(OCH_3)_2$ intermediate requires the collision of the two Ge-containing intermediate species, suggesthing that this reaction is more probable with high Ge-injection rate as shown in Figs. 3-4 (a) and 4-5 (a), where the x-value increases with t_{inj} of Ge-precursor.

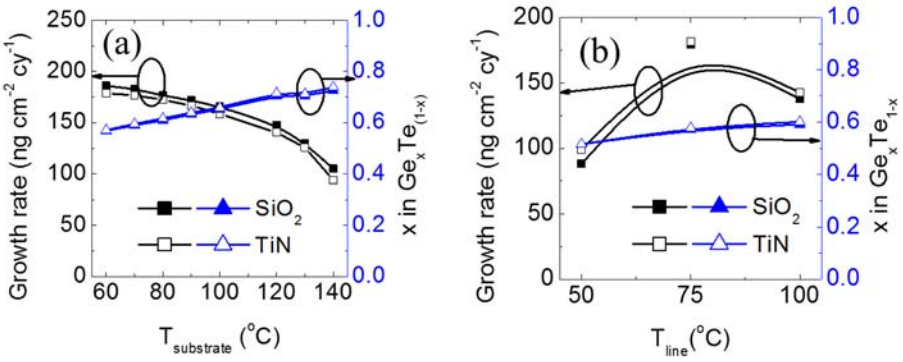

Figure 3-6 Effect of (a) substrate temperature and (b) shared gas flow line temperature where the Ge-precursor and methanol vapor mixture go through.

Next, growth temperature effects were examined for the Ge-canister temperature of 70 °C. In conventional ALD, the optimal temperature range exists where the growth rate is constant, which is known as ALD window. However, based on the complicated reaction mechanisms of intermediate precursors mentioned above, such stable ALD temperature window may not exist. Figure 3-6 (a) shows the growth behavior of $Ge_xTe_{(1-x)}$ at substrate temperatures ranging from 60 to 140 °C. The growth rate of $Ge_xTe_{(1-x)}$ film decreased while the Ge fraction increased with the increasing substrate temperature. Similar decreasing growth rate at an elevated temperature was confirmed in $GeTe_2$ or Sb_2Te_3 ALD using the same Te-precursor,[15] attributable to faster desorption rate of the precursor molecules at high temperature. The increasing x value in $Ge_xTe_{(1-x)}$ with the increasing substrate temperature is assumed to be due to the reaction described in Fig. 3-5 (e) which occurs more actively at higher temperature. The reaction in vapor phase also shows same tendency as can be seen in Fig. 3-6 (b), where the substrate temperature remains constant at 70 °C while the temperature of shared flow line of Ge-precursor and methanol is increased. Owing to the change in growth behavior with temperature, varying compositional films can be easily obtained by controlling the ALD process temperature. For convenience, the process with 5 s of pulse time in Fig. 3-3 (b) whose x value in $Ge_xTe_{(1-x)}$ is close to 0.5, 15 s of pulse time in Fig. 3-4 (a) whose x value is close to 0.6, and temperature at 120 °C in Fig. 3-6 (a) whose x value is close to 0.7 will be referred to as the following: process

A, process B, and process C. The film properties from three different processes were investigated.

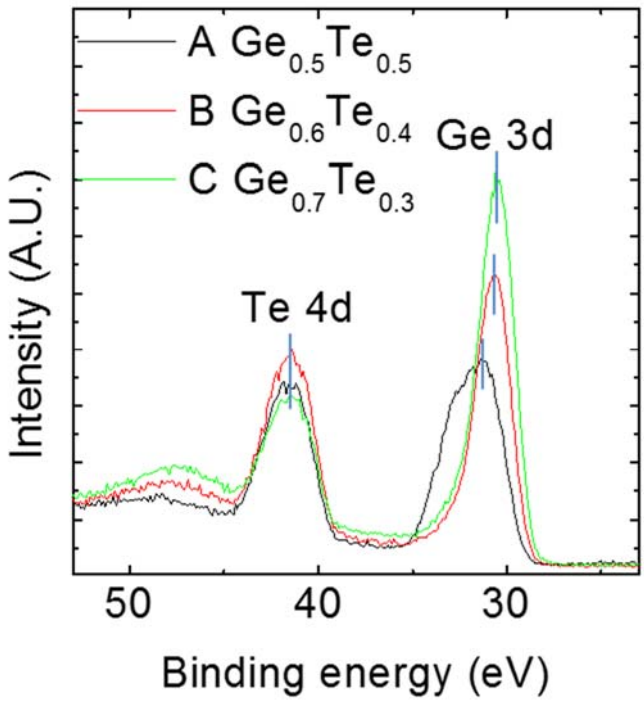

Figure 3-7 X-ray photoelectron spectroscopy results by different deposition process, A; 5 s pulse chosen in Fig. 3-3 (b), B; 15 s pulse chosen in Fig. 3-4 (a), and C; 120 °C temperature was chosen in Fig. 3-6 (a)

In order to validate the suggested model in Fig. 3-5, chemical states of the elements in films were analyzed through synchrotron X-ray photoelectron spectroscopy. Figure 3-7 shows the XPS results of as-deposited films by process A, B, and C, respectively, covering Ge 3d and Te 4d peaks. The photon energy was set as 650 eV, and the surface of the film was cleaned by Ar+ ion sputtering for 5 s. The Ge 3d binding energy of three films were found near 30 eV, higher than Ge crystal of 29.1 eV,[27] which indicates the presence of Ge-Te bond. It can be noticed that with higher Ge fraction, Ge 3d peak is shifted toward the lower binding energy direction, but Te 4d peak remains at the same binding energy. With higher Ge-precursor injection rate in process B compared to process A, reactions described in Figs. 3-5 (d) and (e) occur more frequently owing to the increased amount of the Ge-precursor molecule. Thus, the increase in Ge-Ge bond within the film causes XPS peak to shift towards lower binding energy state. This also applies to process C of which the substrate temperature was higher than process B. On the other hand, the chemical environment of Te atoms remained invariant regardless of the film composition as shown in Te 4d peak in Fig. 3-7; one Te atom always binds with two nearby Ge atoms. Phase diagram of bulk Ge-Te system shows that the non-stoichiometry ranges of Ge and Te are only ~1 atomic%, suggesting that the excess Ge and Te must be segregated as pure Ge or Te phases. However, based on XPS result, no phase separation was observed in as-deposited condition even for the highly non-stoichoimetric composition such as $Ge_{0.7}Te_{0.3}$. This is due to the fact that the

growth temperature is too low to secure the thermodynamic phase stability, but the phase evolution of the film follows the reaction mechanism described in Fig. 3-5. The peak intensity of Ge 3d of process A near 32 eV can be assigned as peak of Ge^{4+} oxidation state. Since the film surface was sputter-cleaned and no significant oxygen signal was found, this intensity can hardly be assigned to GeO_2. Therefore, it must be concluded that the film contains non-negligible concentration of $GeTe_2$, wherein the Ge has +4 oxidation state. This means that there must also be contribution from the phase containing excess Ge, i.e., Ge_2Te, making the overall Ge:Te ratio 1:1. This is also consistent with the XPS results of process A where the Ge 3d peak intensity at binding energy of 30 eV was also rather significant. These findings indicate that the formation of the various intermediate molecules through the reaction pathways indicated in Fig. 3-5 always occurs irrespective of the detailed deposition conditions. The precise film composition appeared to be determined by the relative activity of each reaction.

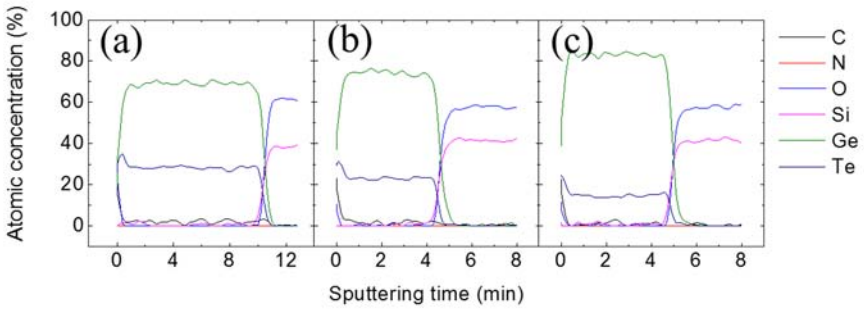

Figure 3-8 Auger electron spectroscopy result by process A, B, and C (each process condition was described in Fig. 3-7)

Figure 3-8 shows the depth-profiling AES result of the films deposited using process A, B, and C, respectively. Elements contained in the precursors, e.g., carbon, oxygen, nitrogen, silicon, germanium, and tellurium were analyzed, and the thickness of the films were 200, 100, 100 nm for process A, B, and C. The analysis confirmed low impurity level under maximum 4 % for all films under examination. It should be noted that the atomic concentration in Fig. 3-8 was not very well calibrated due to the absence of appropriate reference, so only relative variations have significance, and the trend of Ge and Te concentration for the three samples well follows the composition analysis by XRF.

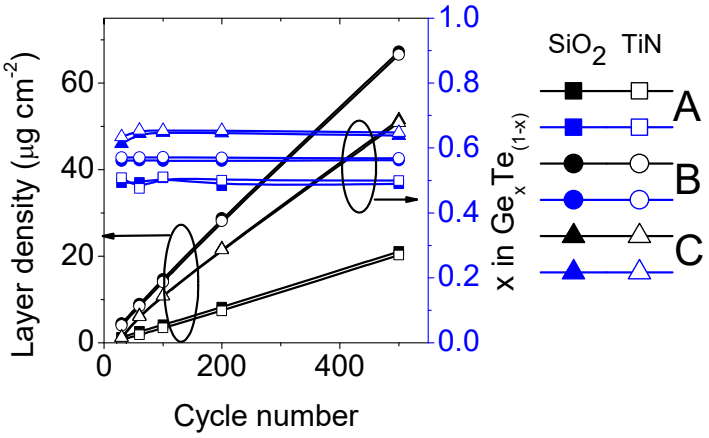

Figure 3-9 Linear growth behavior and constant composition of films deposited by process A, B, and C.

Figure 3-9 presents the linearity of growth behaviors of process A, B, and C as a function of cycle number. Each process shows reproducible and linear growth behaviors and constant film composition except for the first several tens of cycles. From the slopes of the best-linear-fitting graphs, the process A exhibited a relatively low growth rate of 41.6 ng cm^{-2} cy^{-1} (0.75 Å cy^{-1}, considering the density of the film, shown in Fig. 3-10 below). However, using higher precursor injection rate, processes B and C showed 2~3 times faster growth rate of 132.6 ng cm^{-2} cy^{-1} (2.57 Å cy^{-1}) and 103.5 ng cm^{-2} cy^{-1} (2.01 Å cy^{-1}), respectively. The incubation cycle can be deemed negligible from the extrapolation of the data to cycle number = 0. 2.57 Å cy^{-1} is an extraordinarily large growth rate for an ALD process. However, the unit cell parameter of rhombohedral GeTe structure is 5.988 Å[28] so it might be possible to achieve such high growth rate from the ALD process adopted in this work.

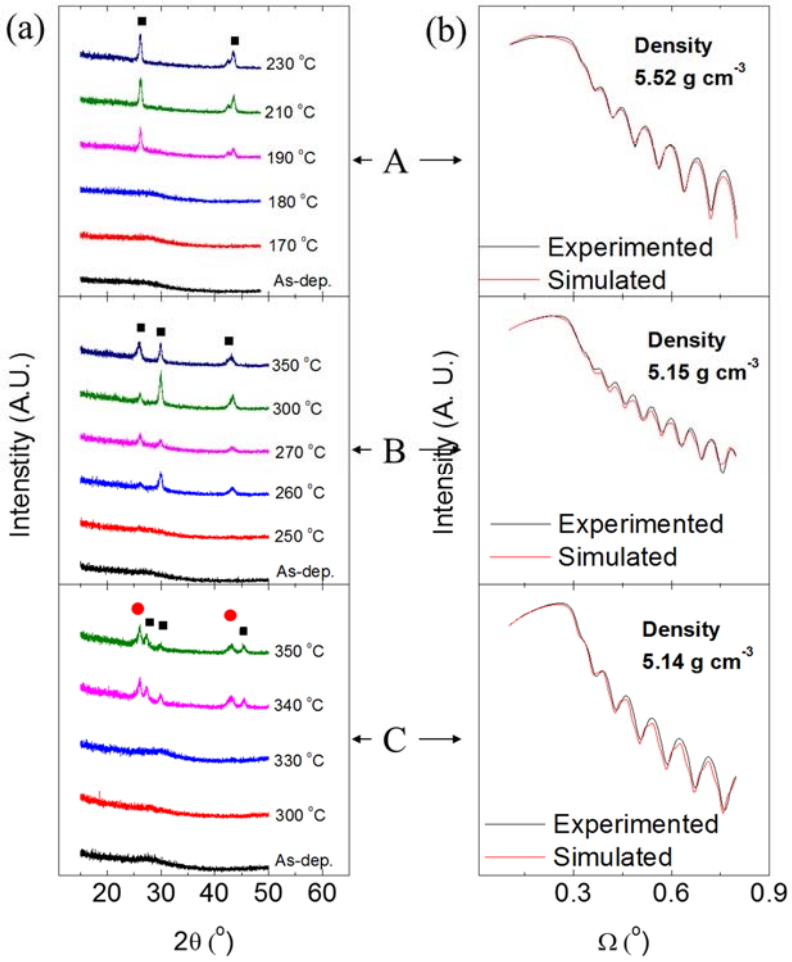

Figure 3-10 (a) Glancing angle X-ray diffraction pattern of as-deposited or annealed films deposited by process A, B, and C for confirmation of crystallization temperature. Peaks were marked by black square from GeTe crystal and by red circle from Ge crystal. (b) X-ray reflectivity results of as-deposited films by process A, B, and C for checking density of films.

Furthermore, additional analysis of GeTe films were performed to evaluate their feasibility as PCM. Figure 3-10 (a) shows the glancing angle XRD patterns of as-deposited and annealed $Ge_xTe_{(1-x)}$ films deposited by process A, B, and C to confirm the crystallization temperature of them. For this experiment, ~40 nm-thick films were annealed at low atmospheric pressure of nitrogen (5 Torr) for 30 minutes. Every film was amorphous in the as-deposited state, and crystallized at different temperatures. Peaks were marked with black square symbol for GeTe crystal, and with red circle symbol for Ge crystal. $Ge_xTe_{(1-x)}$ film deposited by the process A, close to stoichiometric GeTe, was crystallized at temperature between 180 and 190 °C into a rhombohedral phase. This result corresponds well with the crystallization temperature of GeTe film as 185 °C reported by Fantini, et al.[29] Films deposited by the process B and C have much higher crystallization temperature, which is consistent with the results reported by Ge-rich $Ge_xTe_{(1-x)}$ films deposited by RF magnetron co-sputtering.[30] Film by process B was crystallizaed at temperature between 250 and 260 °C. For process C, the film was crystallized at temperature between 330 and 340 °C, and phase separation to Ge/GeTe was observed. Although films generated by process B were also Ge-rich composition, no Ge crystal peak was observed, which might be acribed to the very fine Ge phases if any. Figure 3-10 (b) shows the experimental XRR spectrum and its simulation results for an as-deposited films, showing that density of the film was 5.52, 5.15, and 5.14 $g \cdot cm^{-3}$, respectively. For process A, the film was dense in spite of low deposition

temprature, close to 5.61 $g \cdot cm^{-3}$ which is the theoretical density of amorphous GeTe calculated by Akola, et al.[31] In comparison, Ge-richer compositional films attained by process B and C have relatively low density which is consistent with the fact that Ge is a much lighter element than Te.

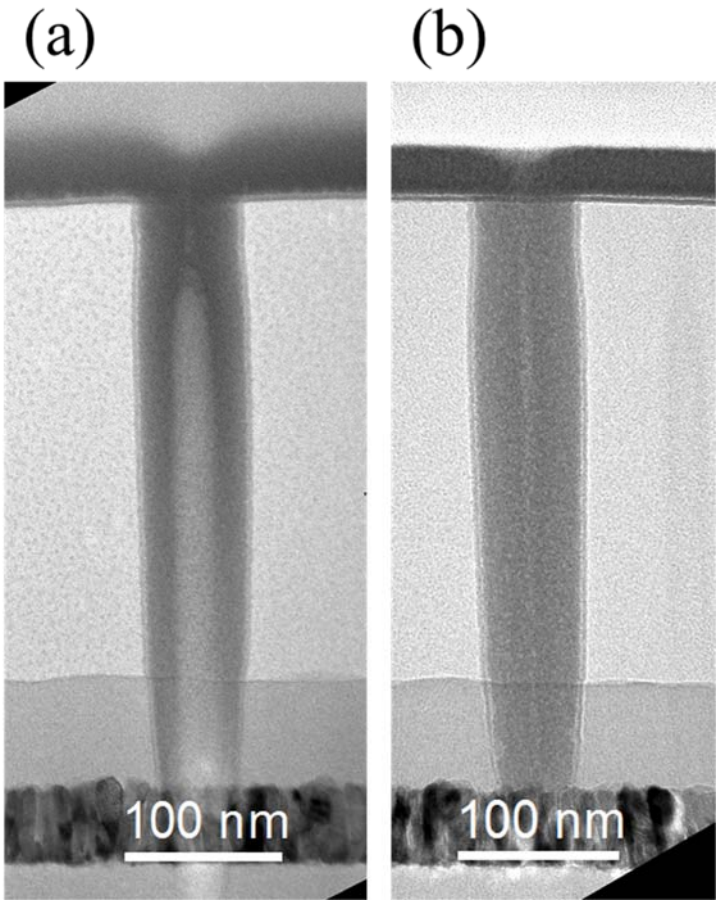

Figure 3-11 Cross-sectional transmission electron microscopy image of film deposited by (a) process A and (b) B on hole whose diameter of 65 nm and aspect ratio of 1:5

Figures 3-11 (a) and (b) show the cross-section TEM images of the films by process A and B, respectively, deposited on hole structure with an opening diameter of 65 nm and aspect ratio of 1:5. For process A, 450 cycles of film was deposited in order to create 40 nm film, which is thick enough to fill the hole structure. However, the cross-section of TEM images showed low conformality and empty volume was observed at the middle portion of the hole structure. This can be easily understood by the insufficient amount of precursor for large surface area of the hole due to unsaturated condition which causes lower growth rate on deeper part of the hole. Essentially, the hole cannot be filled beacause the opening of the hole becomes narrower and eventually closed throughout the deposition. As a result, thinner layer was deposited within the hole instead of the desired 40 nm. For process B, on the other hand, much better conformality of film can be expected due to its saturation behavior. To ensure sufficient injection of the precursor over the larger surface area of hole strucutre than the planar substrate, 20 s of pulse time was chosen from the results in Fig. 3-4 (a), with deposition cycles of 100 to create 25-nm thick film. Figure 3-11 (b) shows superior conformality of process B compared to process A.

Combined process with previously settled Sb_2Te_3 process was attempted for ternary GeSbTe films. Because the saturation condition of the GeTe film does not guarantee stoichiometric GeTe, the final composition of the ternary film should not lie on the GeTe-Sb2Te3 tie line. In the Sb_2Te_3 deposition process, the Sb-precursor react with the Te-precursor to make stoichiometric Sb_2Te_3 film. On the other hand, in the GeTe deposition process, methanol vapor was adopted to form the intermediate Ge- and Te-precursors. At the boundary of GeTe and Sb_2Te_3 processes, the Sb-precursor and the intermediate Te-precursor (or the intermediate Ge-precursor and the Te precursor) reacts which does not occur in the binary deposition processes. Therefore, the reactions in the combined process would be more complicated than binary deposition processes and difficult to study its deposition mechanisms.

To check the effect of various chemical species during the ternary deposition process, effect of methanol vapor on binary Sb_2Te_3 process was tested. Figure 3-12 (a) shows Sb-Te sequences with or without methanol co-injection. As the result can be seen at Fig. 3-12 (b), the final composition of the film was slightly shifted to Te-richer value. This can be understood that methanol vapor also affect on the Sb-Te deposition although the accurate mechanism was not clear yet.

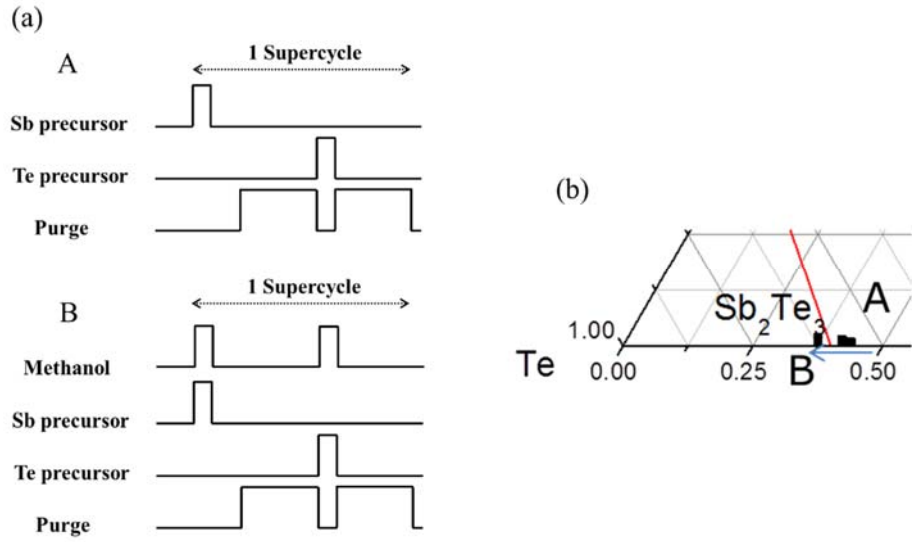

Figure 3-12 (a) Sequence A and B for Sb-Te deposition with/without methanol co-injection, respectively. (b) Composition shift due to effect of methanol vapor

After confirming methanol vapor also affects in the Sb-Te deposition process, combined Ge-Te/Sb-Te process was attempted for ternary GeSbTe films. Baseline recipe was prepared combining saturation condition in each binary Ge-Te and Sb-Te deposition process. Figure 3-13 displays effect of each precursor pulse/purge step modulating only one step time in baseline recipe.

Figure 3-13 (a) shows growth behaviors on SiO_2 substrate during the Sb- and Te-precursor pulse/purge times. Although Sb purge and Te pulse/purge times show saturation behavior, that was not observed during Sb pulse time showing monotonic increasing of Sb-amount during long time as 20 s. Because 5 s of Sb pulse was enough for saturation in binary Sb-Te process, this behavior supports another reaction rather than expected reaction between Sb- and Te-precursors. Unsaturation behavior can be also seen during Ge pulse time in Fig. 3-13 (b). As aforementioned above, the combined deposition process includes too many kinds of chemical species, not only the original form of the precursors, but also its various intermediate precursors. Thus, further mechanism study for the ternary deposition process has limitation for its chemical complexity. Nonetheless, important further experiment was attempted for coverage at composition diagram that changing Sb-Te and Ge-Te sub-cycle ratio.

(a)

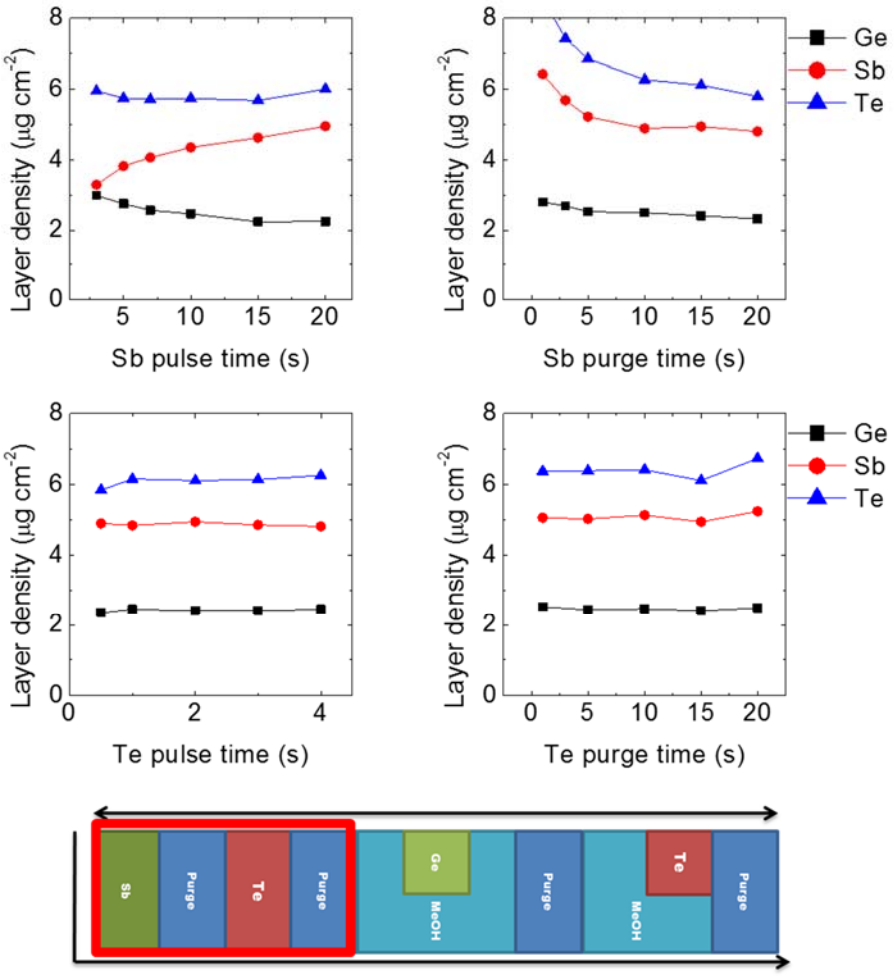
Layer density (μg cm-2)
Sb pulse time (s)
Sb purge time (s)
Te pulse time (s)
Te purge time (s)
Ge
Sb
Te
Sb
Purge
Te
Purge
Ge
MeOH
Purge
Te
MeOH
Purge

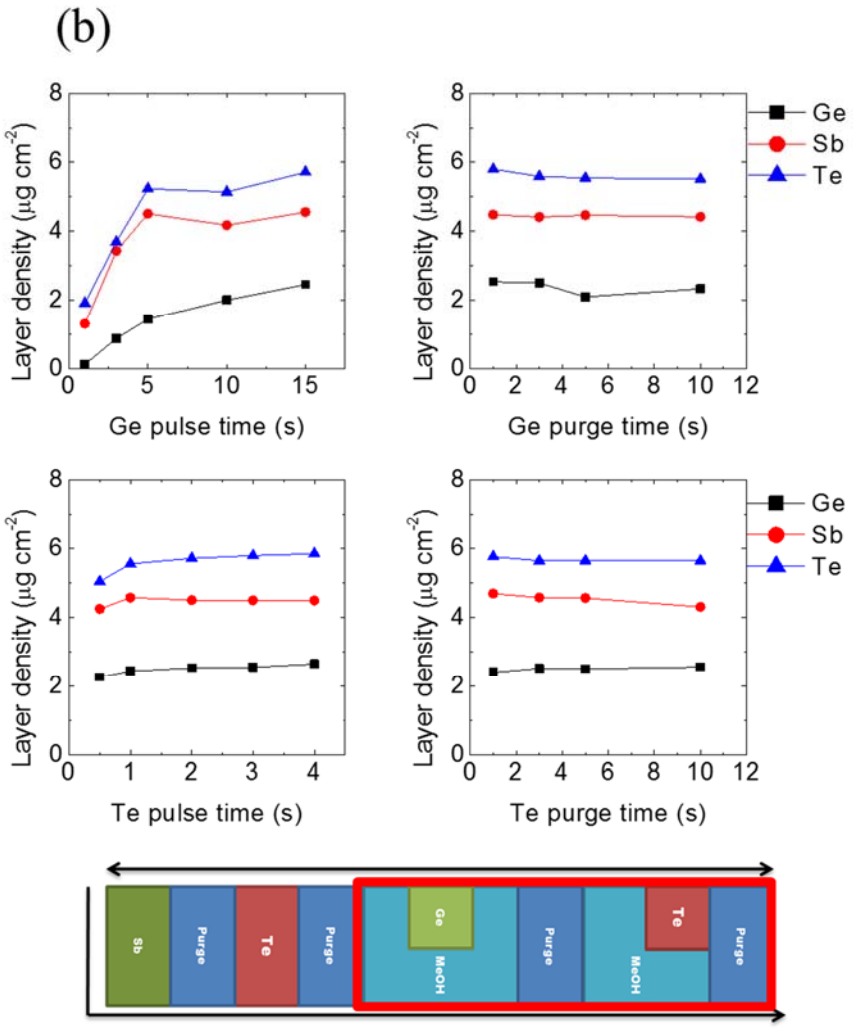

Figure 3-13 Growth behavior during each step in (a) Sb-Te sequence and (b) Ge-Te sequence.

Figure 3-14 shows effect of Sb-Te and Ge-Te sub-cycle ratio during the ternary deposition process. The binary deposition processes were represented as ST and GT, and the combined processes were marked for its sub-cycle ratio. As can be seen in the figure, the composition does not lie on the GT-ST line, but the points consist curved line. This is also can be another supporting data for unexpected reaction because independent depositions of Ge-Te and Sb-Te films occur, the composition should lie on the straight line connecting GT and ST points. However, the results say that other reactions are taking place at the boundary of the sequences.

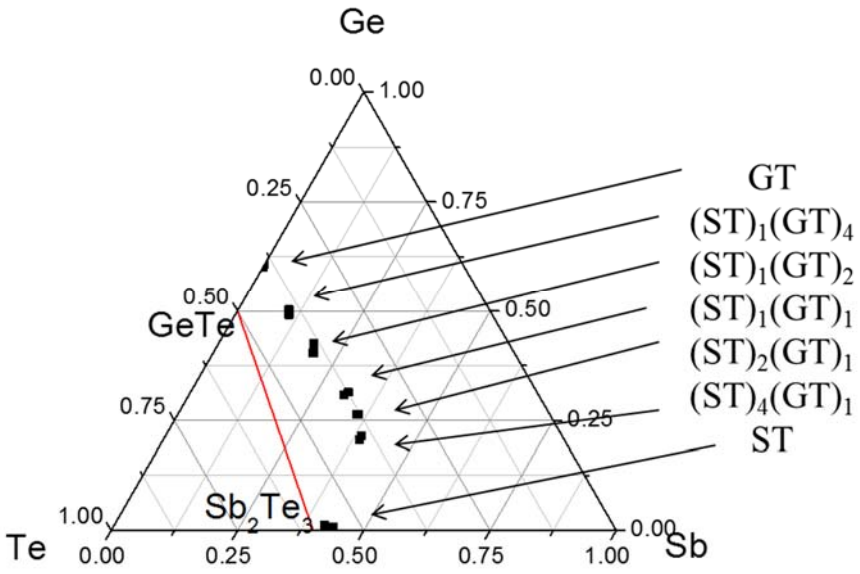

Figure 3-14 Effect of Sb-Te and Ge-Te sub-cycle ratio on ternary GeSbTe deposition.

3.4. Summary

In conclusion, a low temperature (typically 70-120 °C) ALD process to deposit GeTe film was developed using metalorganic precursors: ($Ge(N(Si(CH_3)_3)_2)_2$, $((CH_3)_3Si)_2Te$), and methanol. There was no reaction between $Ge(N(Si(CH_3)_3)_2)_2$ and $((CH_3)_3Si)_2Te$. From the preliminary experiments, it was concluded that formation of intermediates such as $Ge(OCH_3)_2$ and H_2Te, through their chemical reaction with methanol in the gas phase, was necessary to deposit the films. Nonetheless, due to additional reaction between the intermediate Ge-precursor and methanol vapor, the changes in Ge-Te composition was observed. Various compositions of film can be obtained including desired $Ge_{0.5}Te_{0.5}$ by controlling the deposition temperature and the injection rate of the precursor. The notable intermediate molecules that could be produced by the reaction between the pristine Ge-precursor and methanol included various methoxygermane, which may induce $GeTe_2$, and methoxygermylene, which can induce the desired GeTe. However, further reaction between monomethoxygermylene and trimethoxygermane can produce complicated intermadiate molecules that contain Ge=Ge bonds, such as $H(OCH_3)Ge=Ge(OCH_3)_2$. When such complicated intermediate molecules react with H_2Te, which is the end product of the reaction between the initial Te-precursor and methanol and is directly responsible as the Te-precursor for all the explored ALD reactions in this work, even Ge_2Te can be produced.

Therefore, the film composition in this ALD process was suggested to be determined by the relative ratio of formations of the three possible compounds, $GeTe_2$, GeTe, and Ge_2Te. With the increasing portion of Ge-precursor injection, which is always accompanied with co-injection of methanol, change of forming Ge-rich compound, Ge_2Te, increases and the film composition also becomes Ge-richer. A well-saturated ALD growth at an increased injection rate of Ge-precursor was confirmed when sufficiently high Ge-precursor vapor pressure was confirmed, and its chemical model was suggested. The film property showed their feasibility as the PCM, including crystallization temperature of 180 – 190 °C and high density of $Ge_{0.5}Te_{0.5}$ film, and $Ge_{0.6}Te_{0.4}$ film showed crystallization temperature of 250 – 260 °C with no obvious Ge phase segregation. However, $Ge_{0.7}Te_{0.3}$ film showed an even higher crystallization temperature of 330 – 340 °C with Ge phase segregation. High conformality was also confirmed when sufficiently high Ge-precursor vapor pressure was supplied.

3.5. Bibliography

1. J. F. Scott, *in Ferroelectric Memories* (Springer-Verlag, Berlin, Germany 2000).

2. J. Ye, S. T. Lim, M. Bosman, S. Gu, Y. Zheng, H. H. Tan, C. Jagadish, X. Sun and K. L. Teo, *Sci. Rep.* **2**, 533 (2012).

3. Y. W. Yin, J. D. Burton, Y. M. Kim, A. Y. Borisevich, S. J. Pennycook, S. M. Yang, T. W. Noh, A. Gruverman, X. G. Li, E. Y. Tsymbal and Q. Li, *Nat. Mater.* **12**, 397 (2013).

4. T. D. Onuta, Y. Wang, S. E. Lofland and I. Takeuchi, *Adv. Mater.* **27**, 202 (2015).

5. Z. Wen, C. Li, D. Wu, A. Li and N. Ming, *Nat. Mater.* **12**, 617 (2013).

6. E. Y. Tsymbal and A. Gruverman, *Nat. Mater.* **12**, 602 (2013).

7. M. H. Park, H. J. Lee, G. H. Kim, Y. J. Kim, J. H. Kim, J. H. Lee and C. S. Hwang, *Adv. Funct. Mater.* **21**, 4305 (2011).

8. H. M. Christen, E. D. Specht, S. S. Silliman and K. S. Harshavardhan, *Phys. Rev. B* **68**, 020101 (2003).

9. H. N. Lee, H. M. Christen, M. F. Chisholm, C. M. Rouleau and D. H. Lowndes, *Nature* **433**, 395. (2005).

10. A. I. Khan, D. Bhowmik, P. Yu, S. J. Kim, X. Pan, R. Ramesh and S. Salahuddin, *Appl. Phys. Lett.* **99**, 113501 (2011).

11. D. J. R. Appleby, N. K. Ponon, K. S. K. Kwa, B. Zou, P. K. Petrov, T. Wang, N. M. Alford and A. O'Neill, *Nano Lett.* **14**, 3864 (2014).

12. W. Gao, A. Khan, X. Marti, C. Nelson, C. Serrao, J. Ravichandran, R. Ramesh and S. Salahuddin, *Nano Lett.* **14**, 5814 (2014).

13. V. V. Zhirnov and R. K. Cavin, *Nat. Nanotechnol.* **3**, 77 (2008).

14. G. Catalan, D. Jimenez and A. Gruverman, *Nat. Mater.* **14**, 137 (2015).

15. A. I. Khan, K. Chatterjee, B. Wang, S. Drapcho, L. You, C. Serrao, S. R. Bakaul, R. Ramesh and S. Salahuddin, *Nat. Mater.* **14**, 182 (2015).

16. C. S. Hwang, *Adv. Electron. Mater.* **1**, 1400056 (2015).

17. S. Salahuddin and S. Datta, *Nano Lett.* **8**, 405 (2007).

18. C. M. Krowne, S. W. Kirchoefer, W. Chang, J. M. Pond and L. M. B. Alldredge, *Nano Lett.* **11**, 988 (2011).

19. Y. J. Kim, M. H. Park, Y. H. Lee, H. J. Kim, W. Jeon, T. Moon, K. D. Kim, D. S. Jeong, H. Yamada and C. S. Hwang, *Sci. Rep.* **6**, 19039 (2016)

20. A. Q. Jiang, H. J. Lee, G. H. Kim and C. S. Hwang, *Adv. Mater.* **21**, 2870 (2009).

21. D. J. Kim, J. Y. Jo, Y. S. Kim, Y. J. Chang, J. S. Lee, J.-G. Yoon, T. K. Song and T. W. Noh, *Phys. Rev. Lett.* **95**, 237602 (2005).

22. Y. A. Genenko and D. C. Lupascu, *Phys. Rev. B* **75**, 184107 (2007).

23. R. A. Marcus, *J. Chem. Phys.* **24**, 979 (1956).

24. F. Bernardini and V. Fiorentini, D. Vanderbilt, *Phys. Rev. Lett.* **79**, 3958 (1997).

25. M. Nakada, K. Ohashi, H. Tsuda, E. Kawate and J. Akedo, *in Proc. IEEE Int. Symp. on Applications of Ferroelectrics*, Nara, Japan, 27-31 May 2007, edited by (IEEE, USA, 2007), pp. 528 - 530.

26. M. Li, J. Fortin, J. Y. Kim, G. Fox, F. Chu, T. Davenport, T.-M. Lu and X.-C. Zhang, *IEEE J. Sel. Top. Quantum Electron.* **7**, 624 (2001).

27. A. Cano and D. Jimenez, *Appl. Phys. Lett.* **97**, 133509 (2010).

28. M. Specht, M. Städele, S. Jakschik and U. Schröder, *Appl. Phys. Lett.* **84**, 3076 (2004).

29. J. C. Ranuárez, M. J. Deen and C.-H. Chen, *Microelectron. Reliab.* **46**, 1939 (2006).

30. Y.-C. Yeo, T.-J. King and C. Hu, *J. Appl. Phys.* **92**, 7266 (2002).

31. R. H. French, *J. Am. Ceram. Soc.* **73**, 477 (1990).

32. P. V. Thanh, B. N. Q. Trinh, T. Miyasako, P. T. Tue, E. Tokumitsu and T. Shimoda, *Ferroelectrics Lett.* **40**, 17 (2013).

33. J. Junquera and P. Ghosez, *Nature* **422**, 506 (2003).

34. R. Meyer, J. R. Contreras, A. Petraru and H. Kohlstedt, *Integr. Ferroelectr.* **64**, 77 (2004).

35. J. Hoffman, X. Pan, J. W. Reiner, F. J. Walker, J. Han, C. H. Ahn and T. Ma, *Adv. Mater.* **22**, 2957 (2010).

36. K. M. Rabe, C. H. Ahn and J. M. Triscone, *in Physics of Ferroelectrics: A Modern Perspective* (Springer, Berlin, Germany 2007)

4. Atomic layer deposition of GeTe and GeSbTe films using $HGeCl_3$, $Sb(OC_2H_5)_3$, and $\{(CH_3)_3Si\}_2Te$

4.1. Introduction

Based on the current semiconductor industry standards, a high-density, fast-operation, and low-energy-consumption non-volatile memory device is required to fill out the performance gap between the dynamic random access memory and the solid-state disc in computers. Phase change random access memory (PCRAM) is one of the strongest candidates for the next-generation non-volatile memory device, which records binary data via the electrical-resistivity difference between the amorphous and crystalline phases of phase change materials (PCMs). PCRAM is focused due to its fast operation, stable data retention, and high scalability. Many different materials were studied for PCM application, and the most widely researched materials were Ge-Sb-Te ternary materials, especially the GeTe-Sb_2Te_3 pseudobinary materials, including those with a $Ge_2Sb_2Te_5$ composition.[1, 2] It has been reported that a material with a GeTe-richer composition has a better data retention property owing to the higher stability of the amorphous phase while a material with an Sb_2Te_3-richer composition has faster operation attributable to its fast crystallization.[3, 4]

In the early stage of the research, a device structure consisting of planar PCM with a small bottom electrode (called “mushroom structure”) was suggested. It is limited, however, by the large operation current due to its low thermal efficiency and thermal crosstalk issue because there is no thermal barrier among the neighbored cells.[5] To address this problem, a confined cell structure was proposed, wherein PCM is filled within a small hole structure.[6] To deposit PCM into such a small-diameter hole structure, a deposition technique with high conformality is indispensable. In this regard, the development of an atomic layer deposition (ALD) technique for PCM is highly needed for PCRAM with a design rule lower than 10 nm scale in the future memory device technology.

Several plasma-enhanced chemical vapor deposition (CVD) or plasma-enhanced ALD results for ternary GeSbTe have been reported, using alkyl or amino precursors.[7-11] These processes, however, had a step coverage degradation issue owing to plasma usage. In addition, the deposition method using direct reaction between the precursors cannot be realized due to the high chemical stabilities of the precursors, which induce lower ALD reactivity towards each other. Pore et al. reported ALD results using chlorine-based Ge and Sb precursors and silyl-based Te precursor,[12-14] and these authors also reported several studies using slightly different precursors.[15-19] Furthermore, some of the authors reported the detailed ALD behavior of $GeTe_2$-Sb_2Te_3 pseudobinary materials using alkoxy Ge and Sb precursors and silyl-based Te precursor: $Ge(OMe)_4$ (or $Ge(OEt)_4$), $Sb(OEt)_3$, and $((CH_3)_3Si)_2Te$, where Me

and Et represent the methyl and ethyl groups, respectively.[15, 17] The chemistry-specific ALD showed superior deposition characteristics although it had a limitation in achieving the desired composition of the materials lying on the GeTe-Sb_2Te_3 tie line. This limitation originated from the tetravalent oxidation state of the Ge precursor, making $GeTe_2$ by exchanging ligands with the divalent Te precursor at a 1:2 ratio. Therefore, finding an appropriate divalent Ge precursor is an important task in this field. In many researches on ALD or CVD for Ge-containing materials, tetravalent Ge(IV) precursors were reported[7-11, 15, 17, 20, 21] because the Ge element is more stable at the +4 oxidation state than at the +2 oxidation state. Ge(II) precursors are prone to making a polymerized chain or ring structure, which is not optimal for ALD.[22] Ge(II) precursors stabilized by adding adducts or adopting bulk ligands were also reported.[13, 23-25] Moreover, a new GeTe ALD approach using the bulk-liganded divalent Ge precursor $Ge(N(Si(CH_3)_3)_2)_2$ was recently reported.[19] Due to its low reactivity, a unique deposition technique was utilized, in which the methanol vapor was co-injected with the Ge precursor, leading to the formation of an intermediate divalent Ge precursor, $Ge(OMe)_2$, within the vapor phase.[19] Such an approach (i.e., in-situ intermediate-precursor generation in the ALD chamber) could be a novel strategy for overcoming some of the complications related with the chemical specificity of certain substances in the course of their synthesis. Nevertheless, the involvement of an unexpected reaction resulting in the Ge-Ge bond within the film was unavoidable, making the final film

composition slightly Ge-rich GeTe. Therefore, another chemistry is necessary to achieve the desired GeTe film and $Ge_2Sb_2Te_5$ films.

In this study, tetravalent $HGeCl_3$ was used for the Ge precursor, which showed a high feasibility for forming another intermediate Ge precursor where the oxidation state of Ge is +2, to deposit a GeTe film. Under the given ALD conditions, the hydrogen chloride elimination reaction of the $HGeCl_3$ precursor resulted in $GeCl_2$ intermediate-precursor formation. The most stable compound of germanium chloride is the tetrachloride form $GeCl_4$; hence, the ALD of GeTe can be complicated even with the new Ge precursor. In the dichloride form, it easily becomes polymerized, making the ALD reaction less facile.[26] In the previous work of Sarnet et al.,[14] the instability of $GeCl_2$ was compensated for by chelating the molecule with dioxane. Dioxane, however, is not environmentally benign; as such, an alternative route was adopted in this work to fully utilize $GeCl_2$. Meanwhile, $HGeCl_3$ was highly stable at room temperature for more than a year within the sealed stainless steel canister, which renders the ALD process highly repeatable. The developed GeTe deposition process was combined with the previously settled Sb_2Te_3 ALD process to obtain a film with the desired GeTe-Sb_2Te_3 tie line composition. As for the previous results with a similar intention but with slightly different precursors, however, the ALD processes of GeTe and Sb_2Te_3 were not completely independent of each other. Rather, there were significant interactions between the incoming precursor and the previously deposited ALD layers, making the

deposited film composition deviate from the tie line connecting GeTe and Sb_2Te_3. Thus, a further investigation was made to examine the reason behind the compositional deviation, and it was found that the Sb within the previously deposited Sb-Te sublayer reacts with the HCl of several other intermediate components containing Cl to form the volatile $SbCl_3$. An in-depth analysis of this matter is also provided.

4.2. Experimentals

GeTe and GeSbTe films were deposited using a showerhead-type ALD reactor with a 6-inch-wafer scale (CN-1, atomic-premium). The deposition stage was maintained at 70°C, except for testing the effect of varying temperatures. The precursors of Ge, Sb, and Te were $HGeCl_3$, $Sb(OC_2H_5)_3$ and $((CH_3)_3Si)_2Te$, respectively. Each of the precursors was contained in a separate stainless steel canister, which was maintained at 3°C for the Ge precursor, at 40°C for the Sb precursor, and at 35°C for the Te precursor. The vapor pressures of $HGeCl_3$, $Sb(OC_2H_5)_3$, and $((CH_3)_3Si)_2Te$ were 30, 1.1, and 1 torr at their respective canister temperatures, and those at 70°C were 700, 5.0, and 8.0 torr. The thermally evaporated vapor of the Ge precursor was injected in the reactor with 50 standard cubic centimeters per minute (sccm) of Ar carrier gas. Owing to its high vapor pressure, the Ge precursor injection rate was controlled using a metering valve, and no carrier gas was adopted (vapor draw method). The vapors of the Sb and Te precursors were also carried into the reactor by 50 sccm Ar gas. After the precursor injection sequence, 200 sccm Ar gas was used to purge out the excess precursor and byproducts. The process recipes were constructed to induce a reaction between the precursors. For the deposition of the GeTe films, a 100-supercycle precursor sequence was used as the baseline process recipe, as follows: Ge precursor pulse (5 s) – Ge purge (15 s) –Te precursor pulse (2 s) – Te purge (15 s) (Fig. 4-1(a)). Otherwise, it was specified

to check the ALD-type self-limiting behavior. For ternary GeSbTe deposition, the GeTe cycle described above was combined with the Sb-Te cycle: Sb precursor pulse (3 s) – Sb purge (15 s) –Te precursor pulse (1 s) – Te purge (15 s), which is a settled recipe from the previous works.[15] For the mechanism study on Ge insertion into Sb_2Te_3 films, the same injection condition of the Ge precursor was applied on grown Sb_2Te_3 films. SiO_2/Si and TiN/Ti/SiO_2/Si wafers were used as substrates, which had been thermally grown a 100-nm-thick SiO_2 film, a sputtered 50-nm-thick TiN film, and a 5-nm-thick Ti film (called "SiO_2 substrate" and "TiN substrate," respectively). The layer densities of the films were measured via X-ray fluorescence spectroscopy (XRF, Thermo Scientific, Quant'X EDXRF), and the growth rate (GR) was calculated by dividing the layer density by the supercycle number. The impurity level was confirmed via Auger electron spectroscopy (AES, Perkin Elmer, PHI670). The crystallinity and density of the films were measured via glancing angle incidence X-ray diffraction (GAXRD) and X-ray reflectivity (XRR) using an X-ray diffractometer (PANalytical, X'Pert PRO MPD). The step coverage of the film deposited on the hole structure was analyzed via transmission electron spectroscopy (TEM, Tecnai, F20), using a specimen fabricated with a focused ion beam (FIB, FEI, Nova 600 NanoLab).

4.3. Results and Discussions

4.3.1 GeTe film growth

The deposition of GeTe films were conducted though direct reaction between $HGeCl_3$ and $((CH_3)_3Si)_2Te$ based on the following suggested ALD mechanism. $HGeCl_3$ has been known to be easily cleaved into dichlorogermylene and hydrogen chloride, as shown in Equation 4.1.[22, 27] Therefore, it can be readily anticipated that the $GeCl_2$ from Equation 4.1 reacted with the Te precursor to make stoichiometric GeTe through the Equation 4.2.

$$HGeCl_3 \leftrightarrow GeCl_2 + HCl$$

Equation 4.1

$$GeCl_2 + ((CH_3)_3Si)_2Te \rightarrow GeTe + 2\,(CH_3)_3SiCl$$

Equation 4.2

Regarding the chemical equilibrium of equation (1), it was reported that its equilibrium point shifted towards the $GeCl_2$+HCl side at a low temperature, and that even pure $GeCl_2$ can be obtained under suction at -30°C.[27, 28] In this study, the canister temperature of the Ge precursor was maintained at 3°C, and thus, the vapor was expected to consist of $GeCl_2$, HCl, and $HGeCl_3$. During the transfer of the vapor from the cooled canister to the reaction chamber through

the vapor delivery line, however, whose temperature was maintained at 100°C, its equilibrium could have shifted towards the $HGeCl_3$ side. Even so, this shift requires a recombination of $GeCl_2$ and HCl when they collide with each other, and the relatively low chamber pressure (1-2 torr) will not allow such fluent collision. Accordingly, the $GeCl_2$ and $HGeCl_3$ mixture is anticipated to be delivered into the ALD chamber, although the vapor might not be kept at its thermodynamic equilibrium.

To confirm the chemical reactivity between the Ge and Te precursors, film deposition was attempted using the typical ALD sequence shown in Fig. 4-1(a), and the growth behavior during each pulse and purge can be seen in Fig. 4-1(b)-(e). The ALD saturation behavior was observed in each step, and the x value in $Ge_xTe_{(1-x)}$ was maintained at ~0.5 regardless of the pulse/purge times or the growth rate. This is a highly promising result compared with the previous report, in which an attempt was made to grow a GeTe film using a different process, wherein another divalent intermediate $Ge(OMe)_2$ precursor was involved, and it always produced Ge-rich GeTe films.[19] The Ge-rich Ge-Te film composition originated from the unwanted intermediate reaction involving the Ge-Ge bonding in the previous case, but it certainly does not seem to be the case in this work. Hence, it was confirmed that the expected equations (1) and (2) work well throughout the flow line, chamber, and surface of the substrate. Nonetheless, the possible involvement of the uncleaved $HGeCl_3$ into the film

growth cannot be completely discarded, which might have induced $GeTe_2$ due to the tetravalence of Ge in $HGeCl_3$.

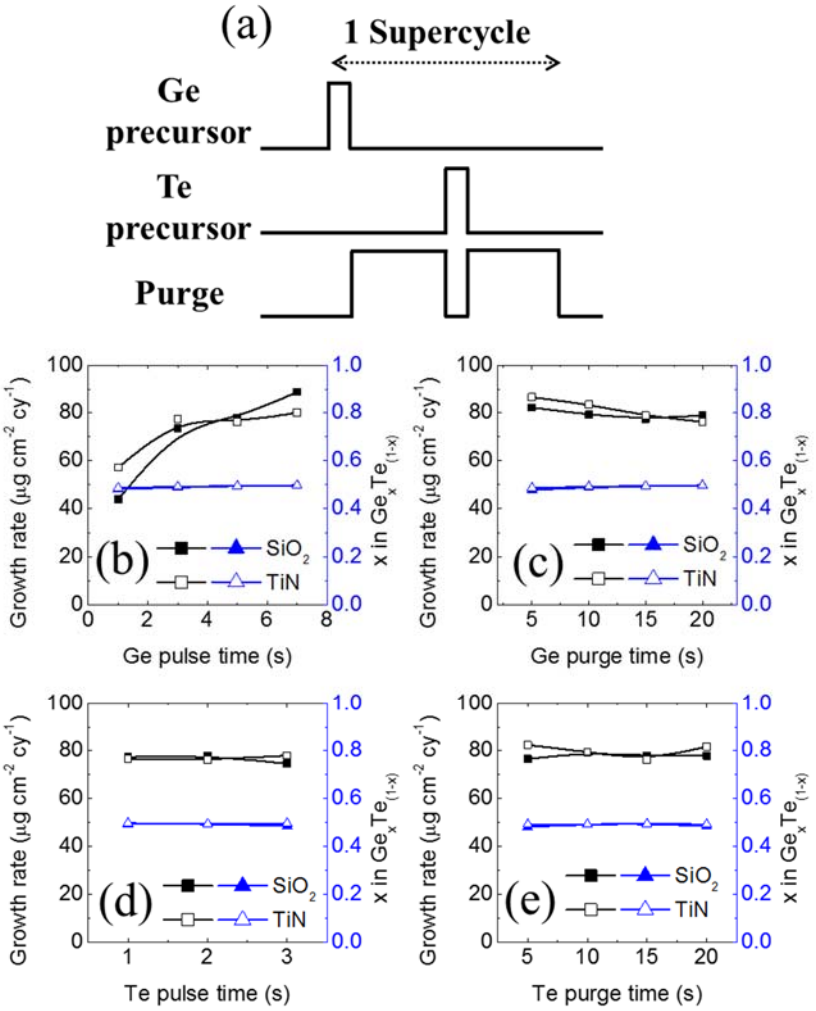

Figure 4-1 . (a) ALD sequence for deposition without process gas. (b)-(d) ALD saturation behavior through the Ge and Te precursors' pulse/purge time split.

To confirm whether or not such adverse reaction can actually take place, the deposition was attempted at varying substrate temperatures. According to Equation 4.1, the concentration ratio between the Ge^{+2} and Ge^{+4} species in the gas phase could be altered at different temperatures, and a higher chamber (or substrate) temperature could have had a higher chance of inducing the involvement of the Ge^{+4} species. If this was the case, the film composition might have been Te-richer as the growth temperature increased. Fig. 4-2(a) shows the effect of the substrate temperature on the deposition using the same ALD sequence, as in the case of Fig. 4-1. The growth rate decreased with the increasing temperature at both substrates, consistent with the previous ALD Ge-Sb-Te films employing different Ge precursors,[15, 19] and the result was due to the faster desorption of the precursor, especially the Te precursor, at a higher temperature. Nonetheless, the x value in $Ge_xTe_{(1-x)}$ was kept constant at 0.5 through the whole temperature range, except for the case at 120°C on the SiO_2 data, where x was ~0.6. The growth rate at this condition was almost zero, making the composition analysis via XRF very unreliable due to its extremely low thickness. Thus, it can be said that within the reliable composition analysis range, all the films showed a stable GeTe composition in spite of the detailed experiment conditions. This finding may indicate the robustness of the suggested ALD mechanism for growing the stoichiometric GeTe film, but it also requires a plausible explanation as to why the direct involvement of $HGeCl_3$ has not occurred. This will be shown in Fig. 4-3.

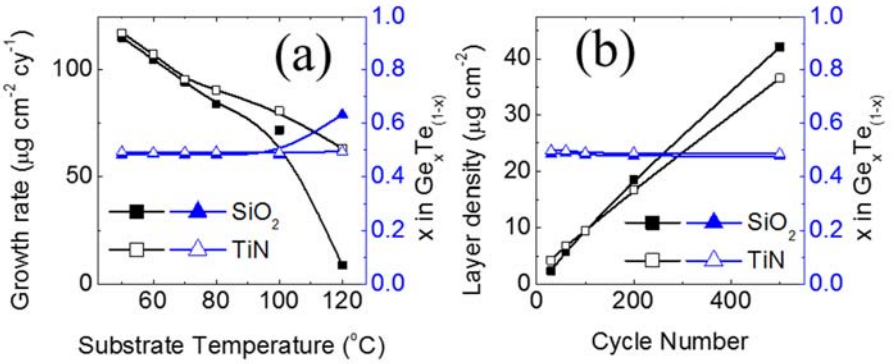

Figure 4-2 (a) Effect of the substrate temperature on the growth rate of the SiO_2 and TiN substrates. (b) Layer densities vs. cycle number to confirm the saturation growth rate and incubation growth behavior.

Fig. 4-2(b) shows the layer densities of the films as a function of the cycle numbers, which are useful for estimating the saturated growth rate and possible involvement of the incubation cycles. Linear growth behaviors were observed on both the SiO_2 and TiN substrates within 30-500 cycles, and the layer density growth rates of 83.5 and 68.3 ng cm^{-2} cy^{-1} were calculated by the slope of the best-linear-fitted graphs on the SiO_2 and TiN substrates, respectively; the values correspond to the thickness growth rates of 0.16 and 0.13 nm cy^{-1}, where the layer density could be converted to thickness through the bulk density estimated from the XRR data to be shown later. These growth rates are reasonable compared to the previous reports on similar materials.[15, 19] The almost zero incubation cycles of the films even on the SiO_2 surface indicate that the nucleation of GeTe was quite fluent. This corroborated the very smooth film surface even after the thick film growth, as will be shown later via AFM examination. The film growth on TiN was even more fluent, as demonstrated by the emergence of a negative x-axis intercept (-40 cycles), meaning that the nucleation of GeTe was highly enhanced on the TiN surface. The film roughness was also very low. The origin of the different saturated growth rate on the two substrates is not yet clearly understood because the deposited-film properties for both substrates, as evidenced by the following analyses, were identical.

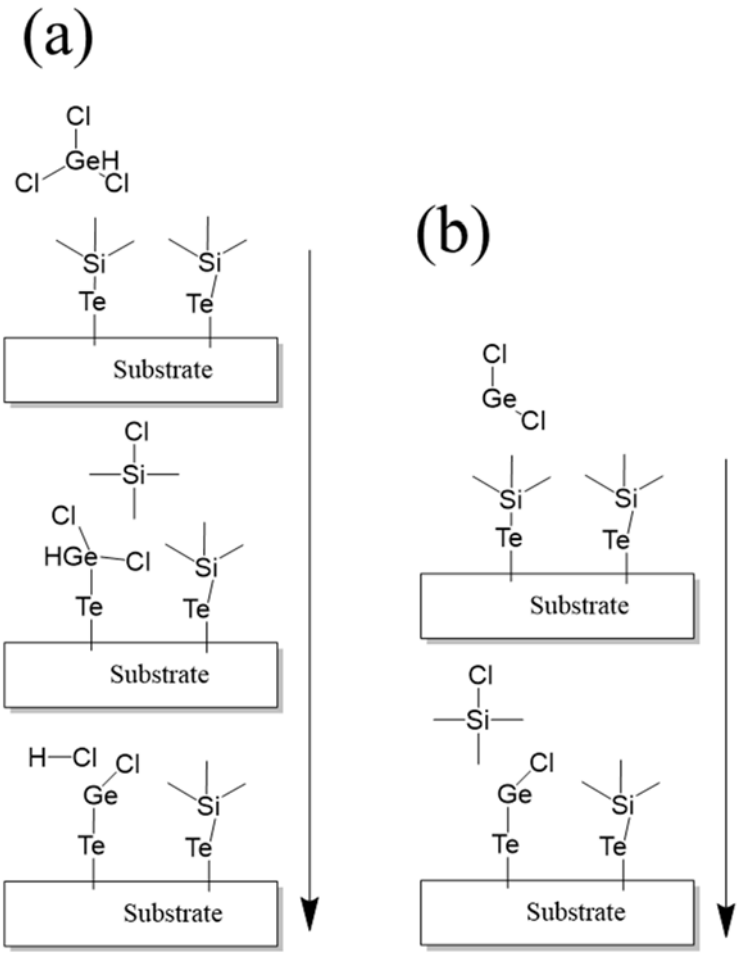

Figure 4-3 Schematic diagrams of the deposition mechanism from (a) $HGeCl_3$ and (b) $GeCl_2$ on the Te precursor terminated surface.

Fig. 4-3 displays the schematic diagram showing the possible mechanisms of stoichiometric GeTe deposition from the delivered $GeCl_2$-$HGeCl_3$ mixture. As mentioned previously, there was a chance that the supplied Ge precursors would have +2 ($GeCl_2$) and +4 ($HGeCl_3$) oxidation states. Fig. 4-3(a) represents the reaction of $HGeCl_3$. The exchange reaction between the chlorine ligand in the Ge precursor and the trimethylsilyl ligand in the Te precursor took place to form HCl_2Ge-Te-. After the exchange reaction, HCl elimination reaction from the reacted species (HCl_2Ge-Te-) was expected to occur more easily than from $HGeCl_3$ because germanium with a Te bond rather than a Cl bond has a weaker bond to the rest of the ligands due to the less-electrophile characteristic of Te compared to Cl.[29] A different path was also possible, wherein the neighboring H-Ge and Cl-Ge would have a ligand exchange to eliminate HCl (schematic diagram not shown). Fig. 4-3(b) illustrates the reaction path of a simpler $GeCl_2$ reaction with the surface silyl-Te species to create a Cl-Ge-Te bond through the same ligand exchange reaction. In both cases, however, GeTe rather than $GeTe_2$ could be achieved, explaining the experiment results of obtaining GeTe for all the deposition conditions. Therefore, $HGeCl_3$ is a very feasible Ge precursor for achieving a GeTe film even if the Ge in it has a tetravalent configuration.

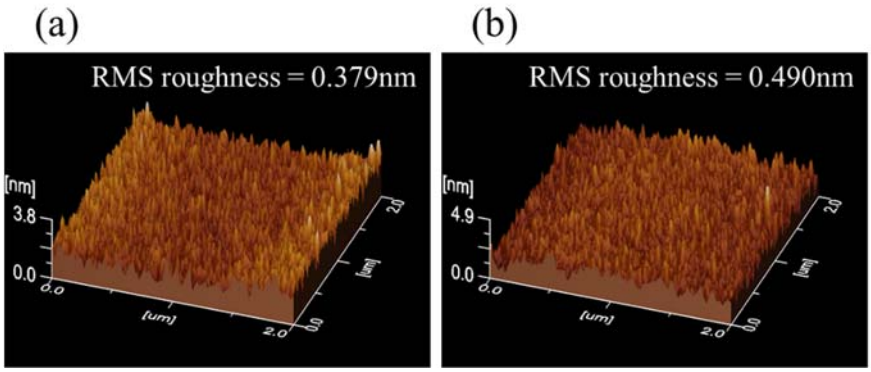

Figure 4-4 AFM images of the samples grown with 500 ALD cycles in Fig. 4-2(b) on a (a) SiO_2 and (b) TiN substrate.

Fig. 4-4(a) and (b) show the AFM topographic images of 78.4- and 68.1-nm-thick films (grown by 500 cycles) on SiO_2 and TiN substrates, respectively, achieving the root-mean-square roughness values of 0.379 and 0.490 nm. The low roughness values corroborate the fluent ALD reaction mechanisms even from the very beginning of the ALD cycles. Fig. 4-5(a) and (b) show the XRR and AES depth profile results of the GeTe film grown by 200 and 1,000 cycles, respectively, on a SiO_2 substrate. The fitting of the XRR results, assuming the GeTe/SiO_2/Si structures of the laminated film, revealed that the film thickness and bulk density were 32 nm and 5.37 g cm^{-3}, respectively. This density value is ~12.5% lower than the density of crystalline GeTe (6.14 g cm^{-3}), and also somewhat lower than the ALD GeTe (5.52 g cm^{-3}) in the previous report.[19] The estimated thickness well matched the expected thickness from the growth rate and number of cycles (0.16 nm cy^{-1} and 200 cycles, respectively). In addition, AES revealed that the film composition was consistent with that of Ge:Te (~50:50) and had good uniformity across the entire film thickness, while impurities like C, Cl, O, and Si were negligible within the film. The significant C concentration on the surface was due to contamination, and it is also quite notable that the O concentration on the film surface was quite low, suggesting the high immunity of the film to oxidation.

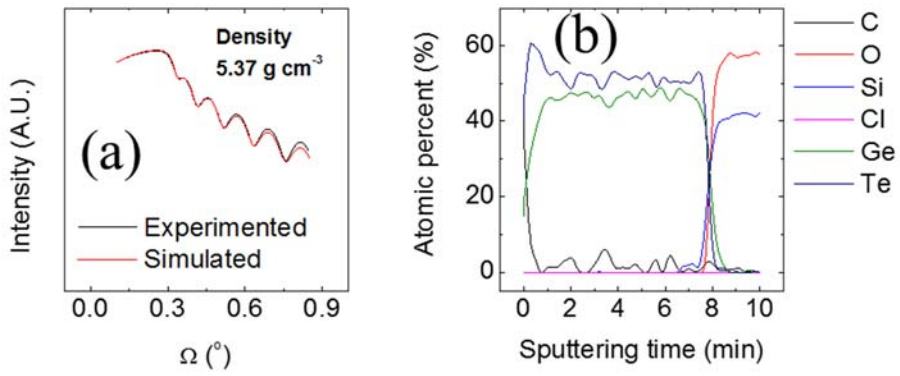

Figure 4-5 (a) X-ray reflectivity result for verifying the density of the film. (b) Auger electron spectroscopy analysis for checking the impurity level and uniformity of the film.

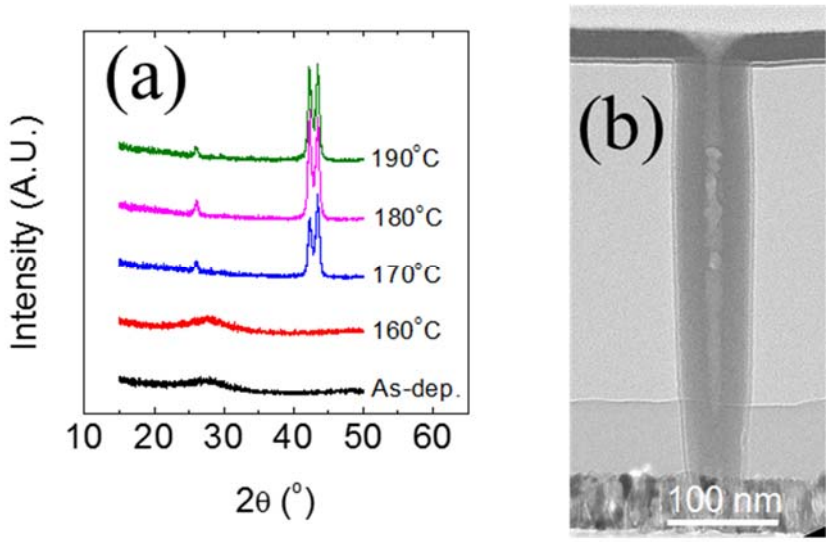

Figure 4-6 (a) GAXRD patterns of the as-deposited or annealed films for checking the crystallization temperature. (b) Cross-sectional TEM image of the films deposited on a hole with a 65 nm diameter and a 300 nm depth.

To confirm the feasibility for phase change application, the crystallization behaviors of the films were analyzed. Fig. 4-6(a) shows the GAXRD results of the as-deposited and annealed films to determine the crystallization temperatures of the films. The 500-ALD-cycle baseline recipe was deposited for 80-nm-thick films on a SiO_2 substrate. The samples were annealed under a N_2 atmosphere at a pressure of 5 torr for 30 minutes. As a result, the films were in an amorphous state at the as-deposited condition but were crystallized into the rhombohedral phase at a temperature over 170°C. This result well corresponds to the crystallization temperature of bulk GeTe (170°C),[30] although it was slightly lower than that of the ALD GeTe films in the previous report. Fig. 4-6(b) shows the cross-section TEM image of the film deposited on a 65-nm-diameter hole pattern with a 1:5 aspect ratio (in the chemical-vapor-deposited SiO_2 layer). The highly uniform film over the entire volume of the hole region demonstrates the excellent step coverage of the process. Next, the GeTe ALD process was combined with the previously developed Sb_2Te_3 ALD process to achieve $Ge_2Sb_2Te_5$ (GST225) films.

4.3.2. $Ge_2Sb_2Te_5$ film ALD

ALD of the GST films with compositions lying on the GeTe-Sb_2Te_3 tie line was attempted by combining the aforementioned GeTe and Sb_2Te_3 ALD processes, which have been described in detail[15] in the authors' previous report, using $Sb(OC_2H_5)_3$ and $((CH_3)_3Si)_2Te$ as Sb and Te precursors. For the deposition, the ALD sequence was employed with the recipe described in Fig. 4-7(a): Sb precursor pulse – Sb purge –Te precursor pulse – Te purge –Ge precursor pulse – Ge purge –Te precursor pulse – Te purge. The process time of Sb precursor pulse – Sb purge –Te precursor pulse – Te purge (Sb_2Te_3) was 3-15-1-15 seconds, which has been identified to be a well-established condition for the saturated growth behavior for the binary Sb_2Te_3 or ternary $GeTe_2$-Sb_2Te_3 ALD process.[15] For the Ge-Te cycle, the same baseline recipe GeTe deposition, 5-15-2-15 seconds for each step, was adopted, and each process time was varied while other times were fixed to confirm the ALD saturation behavior for the GST film growth. Pseudobinary GeTe-Sb_2Te_3 compositional film formation was expected to proceed from Equation 4.2 during the Ge-Te cycle, and from Equation 4.3 during the Sb-Te cycle.

$$2\ Sb(OC_2H_5)_3 + 3\ ((CH_3)_3Si)_2Te \rightarrow Sb_2Te_3 + 6\ C_2H_5O\text{-}Si(CH_3)_3$$

Equation 4.3

Fig. 7(b) and (d) show the growth behavior of each element during each precursor pulse and purge time.

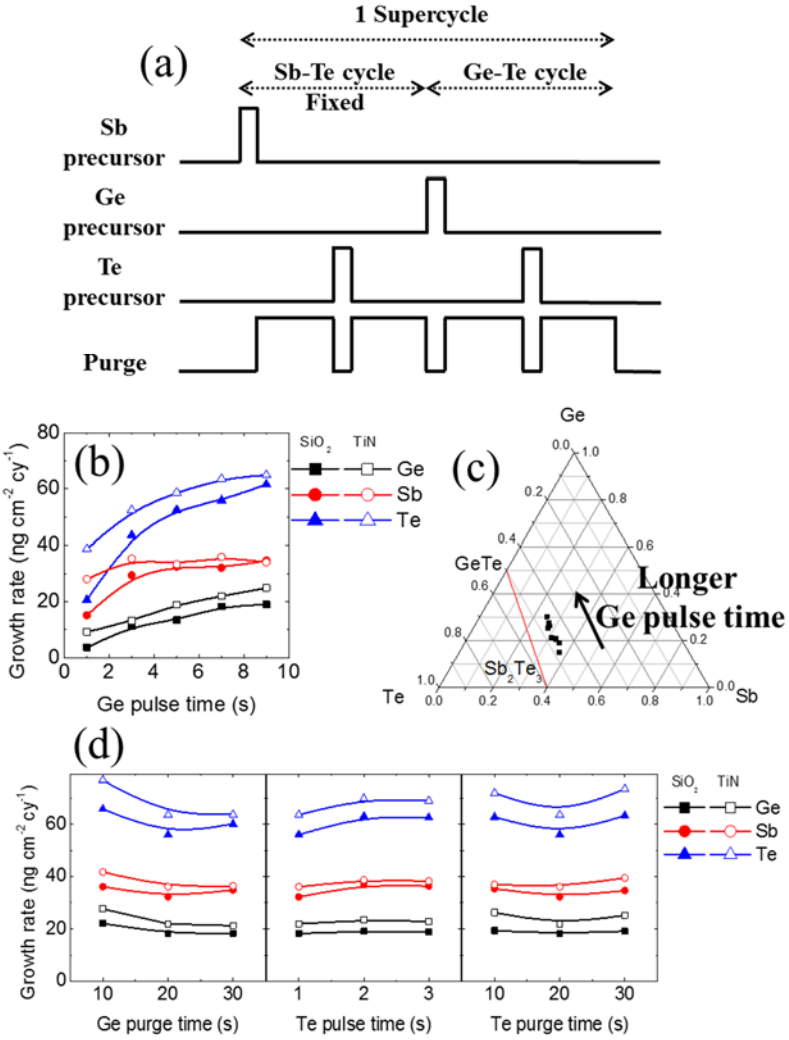

Figure 4-7 (a) Combined process consisting of the Sb-Te and Ge-Te cycles used for ternary GeSbTe deposition. (b) Growth behavior with changing Ge precursor pulse time. (c) Ternary composition diagram for the GeSbTe films in Fig. 4-7(b). (d) Growth behavior with varying Ge precursor purge times and Te precursor pulse/purge times.

In Fig. 4-7(b), the Ge content keeps increasing with the Ge precursor pulse time, without showing the saturation behavior up to a long Ge precursor pulse time of 10 seconds, whereas the saturation could be achieved only at 3-5 seconds in Fig. 4-1(b). A further complication can be seen from the variation in the composition of the films shown in Fig. 4-7(c), which was another interpretation of what was shown in Fig. 4-7(b). If GST films were grown through the simple combination of Equation 4.2 and Equation 4.3, the composition must follow the red line in Fig. 4-7(c). These two unexpected results indicate that there must be an involvement of the unexpected reactions between the precursors or between the precursor and the growing films. The Sb deposition showed a normal saturation behavior, and yet the saturated growth rate was higher than that of Sb_2Te_3, which could be understood from the previous results.[15] During the ALD of the $GeTe_2$-Sb_2Te_3 pseudobinary films, enhancement of Sb_2Te_3 growth on the $GeTe_2$ film compared with that on Sb_2Te_3 itself was observed.[15] Although the involved layer in this work was mostly GeTe rather than $GeTe_2$, a similar enhancement in Sb_2Te_3 growth appears to have occurred. Therefore, it can be concluded that the Sb_2Te_3 ALD proceeded in an ordinary way. The unexpected result of increasing Ge (and Te due to the bonding of the Te precursors with the Ge adsorbates on the film surface) with increasing Ge pulse time up to 10 seconds, however, needs further clarification. To comprehend such incorporation behavior of Ge during the ALD of the GST

films, the following tests were performed under the assumption that the active Ge (intermediate) precursor can react with the Sb atoms in the film.

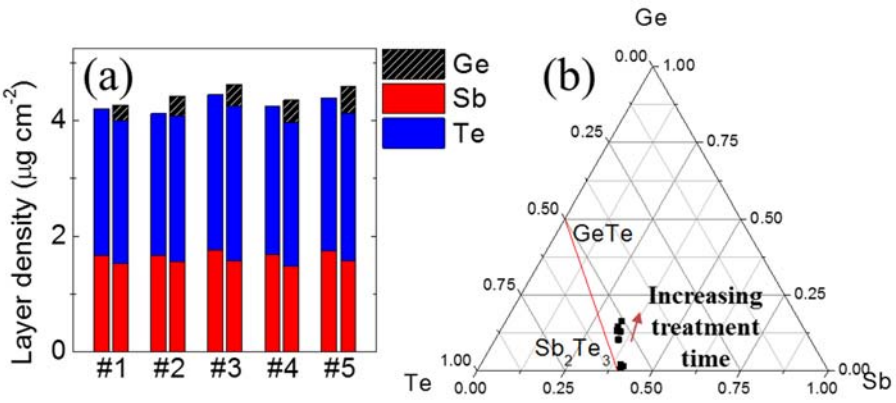

Figure 4-8 (a) Layer densities of the Sb_2Te_3 films deposited with 50 cycles of Sb-Te cycle before/after Ge precursor exposure for 10, 20, 50, 100, and 200 seconds, respectively, for samples 1, 2, 3, 4, and 5. (b) Ternary composition diagram for the films in Fig. 4-8(a).

First, 50 cycles of binary Sb_2Te_3 films were grown. The layer densities of the films were analyzed via XRF (left columns of each set in Fig. 4-8(a)). Next, the samples were again settled into the chamber, to be treated under a Ge precursor vapor environment for 10, 20, 50, 100, and 200 seconds (samples 1, 2, 3, 4, and 5, respectively) at a 70°C substrate temperature. Finally, the layer densities of the samples were checked again to identify the possible differences between before and after the treatment (right columns of each set in Fig. 4-8(a)). It should be noted that the Te precursor injection step was not performed, and as such, there should be no increase in Ge content if no other reactions were involved. The results, however, showed that there was an obvious incorporation of Ge whereas the Sb content decreased. The increase and decrease of the Ge and Sb contents approximately depend on the treatment time. Within the measurement error of XRF, the Te content was demonstrated not to be under the influence of the treatment time. Accordingly, the film composition varied, as described in the ternary composition diagram in Fig. 4-8(b), with the increasing treatment time as indicated by the arrow, and the film composition moved towards the data points displayed in Fig. 4-7(c).

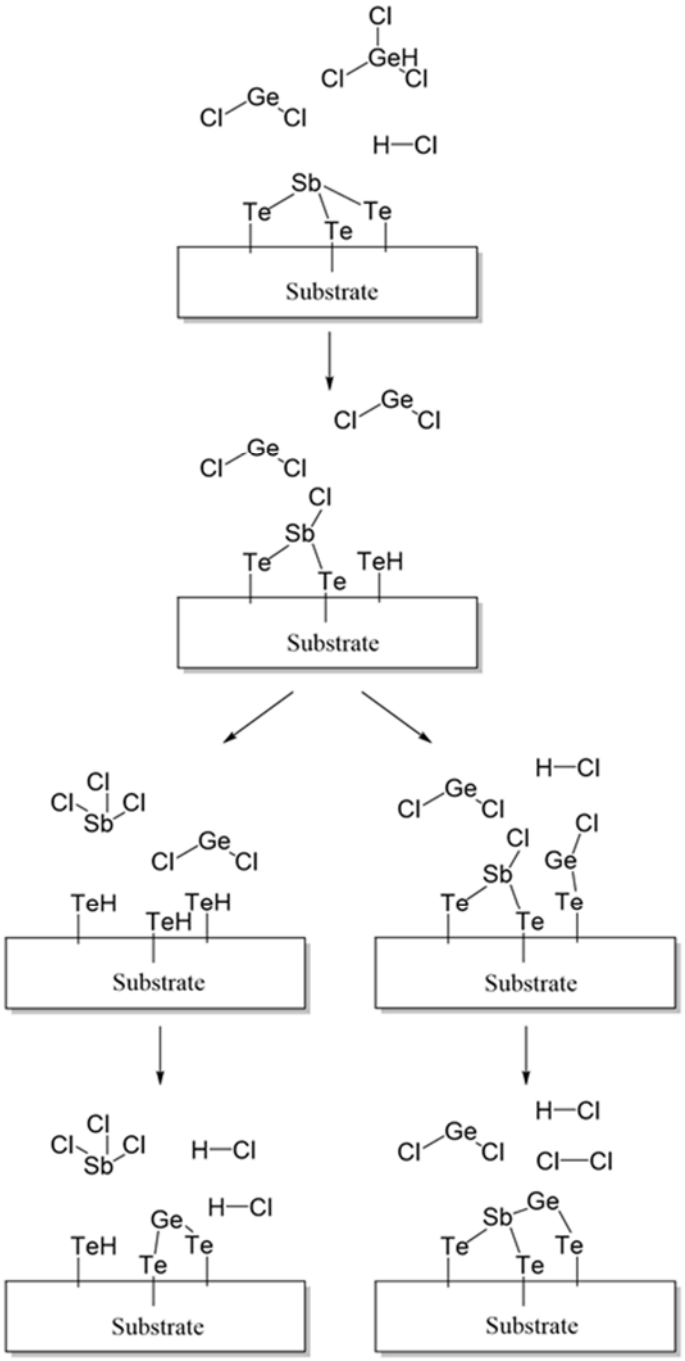

Figure 4-9 Schematic diagram for the mechanism of the Ge insertion reaction during $HGeCl_3$ exposure.

Therefore, it can be conjectured that there is a mechanism that can induce the incorporation of Ge and the removal of Sb during the Ge precursor pulse time. The high chemical reactivity of the Ge precursor may induce a chemical reaction with the already-grown Sb_2Te_3 film, as shown in Fig. 4-9. For clarity, the only probable reaction between the $GeCl_2$ and Sb on the Sb_2Te_3 surface is considered, but an identical reaction mechanism can be executed as the possible reaction between $HGeCl_3$ and the same film, by evolving HCl molecules in addition to the suggested $SbCl_3$ molecule evolution. When highly reactive $GeCl_2$ molecules approach the surface along with the HCl, the Sb atoms in the film may react with the Cl atoms from the HCl to form volatile $SbCl_3$, whereas the H atoms combine with the remaining Te. Then the Te-H site can play the role of the chemisorption site for $GeCl_2$, just as in the usual GeTe ALD process, and Ge can be incorporated into the film while the Sb concentration decreases. The higher stability of $SbCl_3$ compared to $GeCl_2$ may explain the driving force for such adverse reaction.[31] This reaction sequence is represented by the left portion of the reaction flow in Fig. 4-9. Such route can be described as reaction (4):

$$3GeCl_2 + Sb_2Te_3 \rightarrow 2SbCl_3 + 3GeTe$$

Equation 4.4

If this was the only reaction that could occur during the $HGeCl_3$ pulse time, however, the chemical composition of the film must lie on the $GeTe$-Sb_2Te_3 tie line as reaction (4) means that one mole of Sb_2Te_3 is replaced by three moles of GeTe. Therefore, the actual experiment results shown in Fig. 4-7(c) and 8(b) indicate that there must be another mechanism of Ge incorporation into the film. The righthand branch of the reaction mechanism shown in Fig. 4-9 suggests such mechanism. In this case, $GeCl_2$ reacts with Te-H and forms a Cl-Ge-Te species on the surface, while HCl is removed. Therefore, the non-saturating behavior of Ge incorporation with increasing Ge precursor pulse time and deviation of the GST film composition from the ideal tie line can be explained by these surface reaction mechanisms.

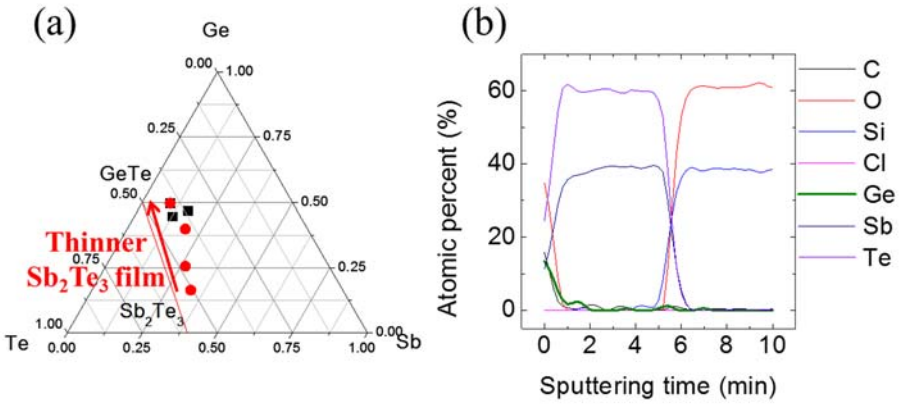

Figure 4-10 (a) Ternary composition diagram for the Sb_2Te_3 films treated with $HGeCl_3$ vapor with different thicknesses and treatment times. (b) Depth profiling Auger electron spectroscopy result of the 5000-second-treated Sb_2Te_3 film deposited through 1,500 cycles of Sb-Te sequence (~90 nm thickness).

Additional experiments were performed for the further understanding of the Ge incorporation process. The thickness of the Sb_2Te_3 films and the treatment times were changed to determine whether the entire Sb_2Te_3 surface or only part of it was converted to GeTe after a long exposure of the Sb_2Te_3 film to the Ge precursor vapor. The results are shown in Fig. 4-10. The solid red circles in Fig. 4-10(a) represent the composition of the films treated for 200 seconds on Sb_2Te_3 films deposited by 10, 20, 30, and 50 Sb-Te cycles, respectively. The red arrow next to the symbols indicates the direction of the thinner Sb_2Te_3 films. Also, the solid black squares in Fig. 4-10(a) present the composition of the films treated for a relatively long time (1000, 2000, and 3000 seconds) on a thin Sb_2Te_3 film deposited through 10 cycles of Sb-Te for confirming the film composition after long treatment times. As can be seen from the solid red circles in Fig. 4-10(a), the atomic percentage of Ge increases as the film Sb_2Te_3 film thickness decreases, suggesting that the surface region of the Sb_2Te_3 film is preferentially changed to GeTe. When the Sb_2Te_3 film was thinnest (~1 nm), almost the entire film seemed to change to GeTe with an Sb concentration lower than ~10%. Even the very long exposure of up to 3,000 seconds, however, did not induce a complete conversion of the film to GeTe (the Sb concentration was still ~10%), meaning that there is an equilibrium between $GeCl_2$ and $SbCl_3$. In addition, the inward diffusion of the Ge-containing species and the outward diffusion of the Sb-containing species at this temperature are somewhat limited, as can be understood from Fig. 4-10(b), which shows the depth profiling AES analysis of

the very thick Sb_2Te_3 film (~90 nm deposited through 1,500 cycles of Sb-Te sequence) after Ge vapor treatment for 5000 seconds.

Referring back to the previous discussion on the ALD process through the combined Ge-Te and Sb-Te sequences shown in Fig. 4-7, the origin of unsaturated growth behavior and the composition disturbance effect was confirmed by the GeTe replacement and Ge addition reactions shown in Fig. 4-9. The ligand-exchange-based ALD reaction and the gas-solid replacement reaction in Fig. 4-9 can be explained in detail as follows. The surface of the growing film right after the Sb-Te sequence will be terminated by the active sites of $–Te(Si(CH_3)_3)$ after the Sb_2Te_3 layer growth. At the beginning of the Ge precursor pulse within the Ge-Te sequence, not only the GeTe formation by Equation 4.2 but also the gas-solid replacement and addition reactions take place. As the reaction kinetics of such additional reactions are limited by the low growth temperature, the reaction increases with increasing Ge precursor pulse time up to 10 seconds, as shown in Fig. 4-7. A similar gas-solid replacement reaction has been reported by some of the authors when the similarly grown Sb_2Te_3 film was treated under the vapor environment of the $((CH_3)_3Si)_3Sb$ precursor.[18] The cracked $(CH_3)_3Si-$ ligands from the Sb precursor react with the Te within the Sb_2Te_3 film, forming volatile $((CH_3)_3Si)_2Te$. This reaction eventually induces the Sb_2Te_3 film to convert to an almost-pure Sb film, which suggests the higher diffusivity of the Sb and Te species within the film.[18] On the contrary, the limited diffusion properties of

the Ge and Sb species in this work rendered only a very thin surface region of the film to be affected by the gas-solid replacement reaction. Nevertheless, during the ALD, the usually-very-thin Sb_2Te_3 layer (<1 nm) caused a substantial portion of the layer to be affected by the reaction.

Due to the involvement of such unavoidable gas-solid interaction during the ALD of the ternary films, it was quite a challenge to grow a GST225 film in this work. Nevertheless, such reaction can be favorably used to modify the film composition of $Ge_2Sb_2Te_7$, which was achieved by the ALD using a more stable Ge precursor with a +4 oxidation state, such as $Ge(OMe)_4$, and identical precursors for Sb and Te, as in this work,[15, 17] towards the composition lying on the desired GeTe-Sb_2Te_3 tie line. Fig. 4-11 shows the experiment results when the 5-nm-thick $Ge_2Sb_2Te_7$ film was treated under a $HGeCl_3$ environment for 10, 20, 30, and 50 seconds, respectively. As mentioned previously, the higher concentration of the Ge/Sb site vacancies of $Ge_2Sb_2Te_7$ compared with that in $Ge_2Sb_2Te_5$ preferably accepted Ge incorporation and film composition changes from the one on the (less desirable) $GeTe_2$-Sb_2Te_3 tie line to the desirable GeTe-Sb_2Te_3 tie line.

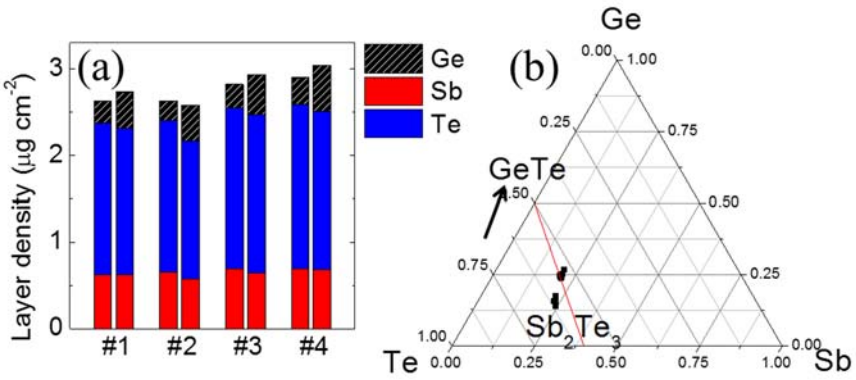

Figure 4-11 (a) Layer densities of the 5-nm-thick $Ge_2Sb_2Te_7$ film before/after Ge precursor exposure for 10, 20, 30, and 50 seconds, respectively, for samples 1, 2, 3, and 4. (b) Ternary composition diagram for the films in Fig. 4-11(a).

4.4. Summary

A novel approach for the Ge precursor for GeTe deposition was suggested using hydrogen chloride elimination reaction of trichlorogermane. $HGeCl_3$ and $((CH_3)_3Si)_2Te$ were used as Ge and Te precursors, respectively, and the films were deposited using direct reaction between the precursors, without any additional process gas. A stable, high-vapor-pressure Ge precursor was presented, which is tetravalent, but its role is closer to being an intermediate $GeCl_2$, and it is supposed to be a feasible divalent Ge precursor for GeTe film deposition. Intriguingly, even the pristine form of $HGeCl_3$, wherein the Ge retains a tetravalent configuration, resulted in the stoichiometric GeTe film. The stoichiometric GeTe ALD process was highly reproducible, and a very feasible ALD-specific saturation behavior was confirmed. The grown GeTe films also showed excellent conformality, with a low impurity level. The film was deposited in the amorphous phase, but it was crystallized at 170°C.

The GeTe deposition process was combined with the Sb_2Te_3 deposition process to obtain a GeTe-Sb_2Te_3 tie line composition. Due to the unexpected reaction, however, between the Ge precursor and the grown Sb_2Te_3 film, a composition slightly deviating from the ideal tie line was obtained. The mechanism for Ge insertion reaction was revealed as the replacement reaction of Sb_2Te_3 into GeTe by chlorination reaction. As a result, the ternary film became Sb-deficient compared with the intended GST225 composition, which

is not an optimum aspect of this precursor chemistry. Nonetheless, it can be favorably combined with the ALD process of $GeTe_2$-Sb_2Te_3, which provided a highly stable ALD platform due to the stable nature of the +4 state of the Ge ions in the precursor, to make the film composition lie on the GeTe-Sb_2Te_3 tie line

4.5. Bibliography

1. Wuttig, M., and Yamada, N., *Nature Materials* **6**, 824-832 (2007).
2. Yamada, N., Ohno, E., Nishiuchi, K., Akahira, N., and Takao, M., *Journal of Applied Physics* **69**, 2849-2856 (1991).
3. Matsunaga, T., Morita, H., Kojima, R., Yamada, N., Kifune, K., Kubota, Y., Tabata, Y., Kim, J. J., Kobata, M., Ikenaga, E., and Kobayashi, K., *Journal of Applied Physics* **103**, (2008).
4. Matsunaga, T., and Yamada, N., *Physical Review B* **69**, (2004).
5. Sadeghipour, S. M., Pileggi, L., and Asheghi, M. In *Phase Change Random Access Memory, Thermal Analysis*, Thermal and Thermomechanical Phenomena in Electronics Systems, 2006. ITHERM '06., San Diego, CA, 2006; IEEE: pp 660 - 665.
6. Cho, S. L., Yi, J. H., Ha, Y. H., Kuh, B. J., Lee, C. M., Park, J. H., Nam, S. D., Horii, H., Cho, B. K., Ryoo, K. C., Park, S. O., Kim, H. S., Chung, U.-i., Moon, J. T., and Ryu, B.-I. In *Highly Scalable on-Axis Confined Cell Structure for High Density Pram Beyond 256mb*, Symposium on VLSI Technology 2005, 2005; IEEE.
7. Choi, B. J., Choi, S., Eom, T., Ryu, S. W., Cho, D. Y., Heo, J., Kim, H. J., Hwang, C. S., Kim, Y. J., and Hong, S. K., *Chemistry of Materials* **21**, 2386-2396 (2009).
8. Choi, B. J., Choi, S., Shin, Y. C., Hwang, C. S., Lee, J. W., Jeong, J., Kim,

Y. J., Hwang, S. Y., and Hong, S. K., *Journal of The Electrochemical Society* **154**, H318-H324 (2007).

9. Choi, B. J., Choi, S., Shin, Y. C., Kim, K. M., Hwang, C. S., Kim, Y. J., Son, Y. J., and HongO, S. K., *Chemistry of Materials* **19**, 4387-4389 (2007).
10. Choi, S., Choi, B. J., Eom, T., Jang, J. H., Lee, W., and Hwang, C. S., *Journal of Physical Chemistry C* **114**, 17899-17904 (2010).
11. Kim, R. Y., Kim, H. G., and Yoon, S. G., *Applied Physics Letters* **89**, (2006).
12. Pore, V., Knapas, K., Hatanpää, T., Sarnet, T., Kemell, M., Ritala, M., Leskelä, M., and Mizohata, K., *Chemistry of Materials* **23**, 247-254 (2011).
13. Ritala, M., Pore, V., Hatanpaa, T., Heikkila, M., Leskela, M., Mizohata, K., Schrott, A., Raoux, S., and Rossnagel, S. M., *Microelectronic Engineering* **86**, 1946-1949 (2009).
14. Sarnet, T., Pore, V., Hatanpaa, T., Ritala, M., Leskela, M., Schrott, A., Zhu, Y., Raoux, S., and Cheng, H. Y., *Journal of The Electrochemical Society* **158**, D694-D697 (2011).
15. Eom, T., Choi, S., Choi, B. J., Lee, M. H., Gwon, T., Rha, S. H., Lee, W., Kim, M. S., Xiao, M. C., Buchanan, I., Cho, D. Y., and Hwang, C. S., *Chemistry of Materials* **24**, 2099-2110 (2012).
16. Eom, T., Gwon, T., Yoo, S., Choi, B. J., Kim, M. S., Buchanan, I., Ivanov, S., Xiao, M. C., and Hwang, C. S., *Chemistry of Materials* **27**, 3707-3713 (2015).

17. Eom, T., Gwon, T., Yoo, S., Choi, B. J., Kim, M. S., Buchanan, I., Xiao, M. C., and Hwang, C. S., *Chemistry of Materials* **26**, 1583-1591 (2014).
18. Eom, T., Gwon, T., Yoo, S., Choi, B. J., Kim, M. S., Ivanov, S., Adamczyk, A., Buchanan, I., Xiao, M. C., and Hwang, C. S., *Journal of Materials Chemistry C* **3**, 1365-1370 (2015).
19. Gwon, T., Eom, T., Yoo, S., Lee, H., Cho, D., Kim, M., Buchanan, I., Xiao, M., Ivanov, S., and Hwang, C., *Chemistry of Materials* (2016).
20. Bosi, M., and Attolini, G., *Progress in Crystal Growth and Characterization of Materials* **56**, 146-174 (2010).
21. Lee, J., Choi, S., Lee, C., Kang, Y., and Kim, D., *Applied Surface Science* **253**, 3969-3976 (2007).
22. Moulton, C. W., and Miller, J. G., *Journal of the American Chemical Society* **78**, 2702-2704 (1956).
23. Kim, S. B., Sinsermsuksakul, P., Hock, A. S., Pike, R. D., and Gordon, R. G., *Chemistry of Materials* **26**, 3065-3073 (2014).
24. Petz, W., *Chemical Reviews* **86**, 1019-1047 (1986).
25. Zemlyanskii, N. N., Borisova, I. V., Nechaev, M. S., Khrustalev, V. N., Lunin, V. V., Antipin, M. Y., and Ustynyuk, Y. A., *Russian Chemical Bulletin* **53**, 980-1006 (2004).
26. Jutzi, P., Hoffmann, H. J., Brauer, D. J., and Kruger, C., *Angewandte Chemie-International Edition in English* **12**, 1002-1003 (1973).
27. Schwarz, R., and Baronetzky, E., *Zeitschrift Fur Anorganische Und*

Allgemeine Chemie **275**, 1-20 (1954).

28. G, B., *Handbook of Preparative Inorganic Chemistry*. Academic Press: New York, 1963; Vol. 2.
29. Parr, R. G., Von Szentpaly, L., and Liu, S. B., *Journal of the American Chemical Society* **121**, 1922-1924 (1999).
30. Caldwell, M. A., Raoux, S., Wang, R. Y., Wong, H. S. P., and Milliron, D. J., *Journal of Materials Chemistry* **20**, 1285-1291 (2010).
31. Cottrell, T. L., *The Strengths of Chemical Bonds*. 2 ed.; Butterworth: London, 1958.

5. Conclusion

GeTe atomic layer deposition processes using novel Ge-precursors have been successfully established. The intermediate precursor formation method was used to make 1:1 compositional GeTe films to overcome instability of Ge(II) precursors. Although the original form of novel precursors has characteristics unsuitable for 1:1 compositional GeTe, this study suggests new way to deposit GeTe films rather than $GeTe_2$ by changing the precursor's characteristics before participating in the reaction.

First, $Ge(N(Si(CH_3)_3)_2)_2$ precursor has too low reactivity towards $((CH_3)_3Si)_2Te$ precursor. To overcome the limitation, intermediate precursors, $Ge(OCH_3)_2$ and H_2Te, was formed by vapor phase reaction with methanol vapor through following Equation 3.2 and Equation 3.4

$$Ge(N(Si(CH_3)_3)_2)_2 + 6CH_3OH \rightarrow Ge(OCH_3)_2 + 2NH_3 + 4CH_3OSi(CH_3)_3$$

Equation 3.2

$$((CH_3)_3Si)_2Te + 2CH_3OH \rightarrow H_2Te + 2CH_3OSi(CH_3)_3$$

Equation 3.4

GeTe films were deposited from these intermediate precursors, through

Equation 3.5:

$$H_2Te + Ge(OCH_3)_2 \rightarrow GeTe + 2CH_3OH$$

Equation 3.5

However, due to chemical complexity of the deposition mechanism, where various chemical species can be produced, unexpected reaction participate in the deposition to deviate the desired 1:1 composition causing Ge-richer composition. Furthermore, the film composition was affected by deposition temperature unlike conventional ALD. However, the study on mechanisms of the deposition process explains the growth behavior very well including the composition issues and saturative growth behaviors. The GeTe deposition process was combined to previously settled Sb_2Te_3 deposition process, however, made composition not lying on the GeTe-Sb_2Te_3 tie line because of

The feasibility on PCRAM application was confirmed by examining physical properties of the film. The film has very low impurity levels of element included in the precursors. The crystallization temperatures of the GeTe films were correspond well to previous reports of GeTe films deposited by different methods. And the films were very dense whose density was very close to theoreticall density of amorphous GeTe.

Second, deposition of stoichiometric GeTe using $HGeCl_3$ and $((CH_3)_3Si_2)Te$ precursors is established wherein Ge element in the Ge-precursor is +4 oxidation state which can cause $GeTe_2$ rather than GeTe. However, hydrogen chloride elimination reaction of the Ge-precursor producing $GeCl_2$ like follwing Equation 4.1 successfully deposits stoichiometric GeTe films thorugh Equation 4.2.

.

$$HGeCl_3 \leftrightarrow GeCl_2 + HCl$$

Equation 4.1

$$GeCl_2 + ((CH_3)_3Si)_2Te \rightarrow GeTe + 2\ (CH_3)_3SiCl$$

Equation 4.2

Unlikely to $Ge(N(Si(CH_3)_3)_2)_2$ precursor, the composition was not affected by deposition conditions such as temperature or precursor pulse times. The stoichiometric GeTe films were also checked for feasibility to PCRAM applications. Depth profiling spectroscopy showed the film deposited by the process has very low impurity levels of carbon, oxygen, chlorine, and silicon. Very smoothe morphology with fine grain was observed comparing to the first process using different precursor. The film was deposited in amorphous phase due to low deposition temperature of 70 °C, and crystallized at 170-180 °C which is well correspond to crystallization temperature of bulk GeTe film from literatures. The process was combined with Sb_2Te_3 deposition process to obtain

GeTe-Sb_2Te_3 pseudobinary, however, slightly deviated from desired composition because of reaction between the Ge-precursor and grown Sb_2Te_3.

- Conventional furnace annealing for ambient and vacuum annealing
- TEM sampling

3. Analysis methods

- X-Ray Fluorescence Analyzer (XRF, Thermo scientific, ART Quant'X EDXRF) for analysis of composition and layer density of film
- X-ray Diffractometer (PANalytical, X'Pert PRO MPD) for measurement of X-ray diffraction, X-ray reflection and reciprocal space mapping.
- Atomic Force Microscopy (AFM, JEOL, JSPM-5200) for analysis of the topography
- Spectroscopic Ellipsometer (SE, J.A. Woollam, M-2000) for analysis of optical properties and thicknesses of thin films
- Four point probe for resistivity measurement of metals and conducting materials
- Pulse/pattern generator (Agilent, 81110A/81111A) and digital oscilloscope for pulse switching measurement of phase-change materials
- HP4140B and HP4145B for I-V measurement of phase-change memory
- Characterizing thin films by XPS, RBS, AES, TEM

4. Programs apprentice

- ChemBioDraw/Chem3D 14

Abstract (in Korean)

현재의 정보화 사회는 빠른 동작 속도, 높은 밀도, 낮은 소비전력의 메모리 장치를 필요로 한다. 그러나 dynamic random access memory (DRAM) 및 NAND flash 로 대표되는 현재의 반도체 산업은 축소화 한계에 도달하였고 차세대 메모리에 대한 연구가 지속되고 있다. 상전이 물질의 비정질 및 결정질 간 비저항 차이를 통해 데이터를 기록하는 상전이메모리는 차세대 비휘발성 메모리의 가장 강력한 후보 중 하나이다. 가장 널리 연구된 상전이 물질은 GeTe-Sb2Te3 계선 상의 물질로, 빠른 상전이, 우수한 데이터 유지 특성, 낮은 전력 소비 특성을 가지고 있다.

한 편, 상전이메모리 연구의 초기 단계에서는 평판형의 상전이물질에 작은 전극 접촉을 형성하는 버섯모양 구조를 사용하였다. 그러나 버섯모양 구조의 상전이메모리는 인접한 셀 간의 간섭 문제 및 낮은 열효율 문제를 가져 개선이 필요하다. 따라서 상전이물질을 작은 구멍에 채우는 새로운 매립형 구조가 제안되었다. 이러한 매립형 구조는 훨씬 높은 열효율, 개선된 인접 셀 간섭 문제 뿐만 아니라 제조 공정 중에 식각 데미지에도 강한 저항성을 가져 상전이메모리의 새로운 표준이 되었다. 이러한 매립형 구조의 상전이메모리 소자를 제조하기 위해서는 우수한 단차피복성 특성을 갖는 증착공정이 중요하게 되었다. 이러한

요구사항에 따라 상전이물질의 원자층증착법 연구가 필요하게 되었다.

삼성분계 GeSbTe 물질의 원자층증착에 대한 이전의 연구는 많은 문제들로 인해 개선해야 할 과제들을 남겼다. GeSbTe 원자층증착법에 대한 앞선 연구들에서 가장 중요한 문제 중 하나는 원하는 조성인 GeTe-Sb2Te3 계선이 아닌 GeTe2-Sb2Te3 계선에 있는 재료가 증착된다는 점이다. 문제의 원인은 -2 가 산화상태의 Te 전구체와 반응할 Ge 전구체가 +4 가 상태에 있어 GeTe 가 아닌 GeTe2 를 형성하기 때문이었다. 이는 Ge 원소의 가장 안정한 산화상태가 +4 이기 때문으로, 이러한 특성은 Ge(II) 전구체의 화학적 불안정성을 야기하여 전구체 개발 및 이를 이용한 증착공정 개발에 많은 어려움이 있었다. 본 연구에서는 GeTe 박막을 원자층증착법으로 증착하는 새로운 공정들이 제시되었다. 두 공정에서 공통적으로, 전구체의 원래 형태와 증착에 참여하는 형태가 다른 중간전구체 형성방법이 새롭게 제안 및 사용되었다.

첫 번째 공정은 Ge 원자가 +2 가 산화상태에 있는 $Ge(N(Si(CH_3)_3)_2)_2$ 및 $((CH_3)_3Si)_2Te$ 전구체가 각각 Ge 및 Te 전구체로 사용하여 개발되었다. Ge 전구체는 챔버로 주입되는 과정에서 메탄올 증기와 기상 반응하여 중간전구체인 $Ge(OMe)_2$ 를 형성하였으며, 이러한 형태로는 폴리머를 형성하기 때문에 장기적인

안정성이 없어 이와 같은 중간전구체 형태로만 사용이 가능하다. Te 전구체 또한 중간전구체 형태인 H_2Te 를 형성하기 위해 메탄올 증기와 함께 주입되었다. 앞서 기술된 중간전구체들은 서로 간의 직접반응을 통해 GeTe 박막을 형성하였다. 이러한 증착 공정에서 발생하는 화학반응에 대한 메커니즘이 연구되었다. 또한, 이전에 확립된 $Sb(OC_2H_5)_3$ 및 $((CH_3)_3Si)_2Te$ 전구체를 이용한 Sb_2Te_3 증착공정과 결합되어 삼성분계 GeSbTe 박막을 증착하는 시도 역시 수행되었다.

$HGeCl_3$ 및 $((CH_3)_3Si)_2Te$ 를 Ge 및 Te 전구체로 사용한 두 번째 공정 역시 제안되었다. 전구체의 원래 형태에서는 Ge 원자가 +4 가 산화상태로 존재하지만 탈염화수소 반응을 통해 HCl 및 $GeCl_2$ 로 분해된다. 분해된 분자는 Te 전구체와의 직접 반응을 통해 화학양론적인 GeTe 를 형성할 수 있는 $GeCl_2$ 형태로 반응에 참여한다. 이 공정은 역시 Sb2Te3 증착공정에 결합되어 GeTe-Sb2Te3 준 이성분계 박막 증착이 시도되었다. 이러한 과정에서 이성분계 GeTe 및 삼성분계 GeSbTe 박막 증착 공정에 대한 메커니즘 연구가 수행되었다.

주요어: 상전이메모리, 원자층증착법, 텔루륨화 저머늄, 텔루륨화 저머늄 안티모니, 증착 기전

학번: 2011-22860

권 태 홍